Title: A New Quantitative Cell Microscopy Approach Reveals Mechanistic Insights into Clearance of Membrane Substrates by the AAA Protein Msp1

Authors: Nicholas R. Weir[1], Roarke A. Kamber[1], James S. Martenson[1], and Vladimir Denic[1,2]

1. Department of Molecular and Cellular Biology, Harvard University, Cambridge, MA 02138 USA

2. Corresponding Author: Vladimir Denic, vdenic@mcb.harvard.edu

SUMMARY

Msp1 is a conserved AAA ATPase in budding yeast localized to the surface of mitochondria where it prevents accumulation of mistargeted tail-anchored (TA) proteins, including the peroxisomal TA protein Pex15. Msp1 also resides on peroxisomes but it remains unknown how TA proteins native to mitochondria and peroxisomes evade Msp1 surveillance. Using new quantitative cell microscopy tools for studying Msp1 function, we observed that a fraction of peroxisomal Pex15, exaggerated by overexpression, is turned over by Msp1. Kinetic analysis and theoretical modeling revealed that mitochondrial Pex15 molecules are all equally susceptible to Msp1. By contrast, peroxisomal Pex15 molecules are converted from an initial Msp1-sensitive to an Msp1-resistant state. Lastly, we show that Pex15 interacts with the peroxisomal membrane protein Pex3, which shields Pex15 from Msp1-dependent turnover. In sum, our work argues that Msp1 selects its substrates on the basis of their solitary membrane existence.

KEYWORDS

Msp1, AAA ATPase, tail-anchored protein, protein quality control

INTRODUCTION

Tail-anchored (TA) proteins are integral membrane proteins with a single C-terminal transmembrane segment (TMS). In the budding yeast *Saccharomyces cerevisiae,* the majority of TA proteins are captured post-translationally by cytosolic factors of the conserved Guided Entry of TA proteins (GET) pathway, which deliver them to the endoplasmic reticulum (ER) membrane for insertion by a dedicated insertase (Denic et al., 2013; Hegde and Keenan, 2011). TA proteins native to the outer mitochondrial and peroxisomal membranes are directly inserted into these membranes by mechanisms that are not well defined (Chen et al., 2014a; Papić et al., 2013, and reviewed in Borgese and Fasana, 2011). Gene deletions of GET pathway components (*getΔ*) result in reduced cell growth and TA protein mistargeting to mitochondria and cytosolic TA protein aggregates (Jonikas et al., 2009; Schuldiner et al., 2008). Two recent studies identified the ATPase associated with diverse cellular activities (AAA ATPase) Msp1 an additional factor for supporting cell viability in the absence of GET pathway function (Chen et al., 2014b; Okreglak and Walter, 2014). Specifically, they observed that *msp1Δ* cells accumulate mislocalized TA proteins in the mitochondria and that double *msp1Δ getΔ* cells have synthetic sick genetic interactions. This sick phenotype is associated with disruption of mitochondrial function and is exacerbated by overexpression of TA proteins prone to mislocalization. Msp1 is a cytosolically-facing transmembrane AAA ATPase which resides on both mitochondria and peroxisomes. Closely-related members of Msp1's AAA ATPase subfamily form hexamers that bind hydrophobic membrane substrates and use the energy of ATP hydrolysis to extract them for protein degradation (Olivares et al., 2016). Several lines of evidence are consistent with the working model that Msp1 operates by a similar mechanism: ATPase-dead mutations of Msp1 are unable to complement *msp1Δ* mutant phenotypes; mitochondrial mistargeting of TA proteins leads to their enhanced co-

immunoprecipitation with ATPase-dead Msp1; cells lacking Msp1 have increased half-lives of mistargeted TA proteins; and lastly, a complementary analysis of the mammalian Msp1 homolog ATAD1 (Chen et al., 2014b) established a conserved role for Msp1 in correcting errors in TA protein sorting.

AAA proteins can share the same intrinsic enzymatic activity but still be subject to different rules of substrate recognition (Olivares et al., 2016). Some insight into Msp1 substrate selectivity comes from negative evidence showing that native mitochondrial TA proteins are inefficient Msp1 substrates (Chen et al., 2014b). Thus, mistargeted TA proteins might contain intrinsic Msp1 recognition determinants, but it is difficult to exclude the possibility that mitochondrial TA proteins are protected from Msp1 recognition by extrinsic mitochondrial factors. In fact, a similar possibility could explain the apparently mitochondria-specific behavior of Pex15 as a substrate. Peroxisomal Pex15 appears to stably co-reside with Msp1 at peroxisomes, but becomes an Msp1 substrate when mistargeted to mitochondria (Chen et al., 2014b; Okreglak and Walter, 2014). Thus, there is circumstantial evidence for the existence of substrate-extrinsic factors specific to mitochondria and peroxisomes that block Msp1 access to native TA proteins at these organelles.

Substrate selectivity mechanisms of many AAA proteins have been successfully dissected by bulk cell approaches for measuring substrate turnover. These approaches are resolution-limited, however, when used to study Msp1 in *getΔ* cells because TA proteins mistargeted to mitochondria co-exist with a dominant TA population that remains correctly localized in the same cell. Previous studies overcame this issue through two different approaches that increased the ratio of mistargeted to properly localized substrates. In one case, cells were engineered to produce a Pex15 deletion

mutant ($Pex15_{\Delta C30}$) that is efficiently mistargeted to mitochondria because it lacks its native peroxisomal targeting signal (Okreglak and Walter, 2014). A major limitation of this approach, however, is its inherent unsuitability for establishing if native Pex15 is a latent Msp1 substrate because of undefined peroxisomal factors. Second, a cell microscopy pulse-chase approach was used to monitor turnover of mitochondrial signal from transiently expressed fluorescently-labeled wild-type Pex15 made susceptible to mistargeting by deletion of *GET3* (Chen et al., 2014b). In this approach, expression of Pex15 was transcriptionally controlled by the inducible *GAL* promoter in cells expressing wild-type, ATPase-dead, or no Msp1. Comparison of mitochondrial Pex15 clearance following *GAL* promoter shut-off revealed that cells lacking functional Msp1 had a reduced fractional rate of substrate clearance; however, these cells also had a larger starting population of mitochondrial Pex15. Because cells expressing functional Msp1 did so during both the Pex15 pulse and chase periods, these results could have been explained by Msp1 only blocking its substrates insertion into the membrane. To determine how Msp1 distinguishes between substrates and non-substrates and to determine if it facilitates substrate extraction or blocks insertion, better tools are needed for temporally controlling and accurately measuring Msp1 activity *in vivo,* which in turn will set the benchmark for future biochemical reconstitutions of Msp1's cell biological function.

Here, we began by devising a synthetic gene system for independent control of Pex15 (either wild-type or $Pex15_{\Delta C30}$) and Msp1 expression with two drugs as transcriptional inducers. Next, we coupled this tool to live-cell confocal microscopy and computational image analysis to quantitate Pex15 signal density separately at mitochondria and peroxisomes. Using this pipeline and a protease-protection assay, we determined that *de novo* induction of Msp1 activity drove

efficient clearance of a Pex15 substrate that was fully membrane-integrated at mitochondria. In the process of dissecting the kinetics of Pex15 turnover at mitochondria, we observed that Msp1 can also eliminate overexpressed Pex15 from peroxisomes, but with a different kinetic profile. Theoretical model fitting revealed that all mitochondrial Pex15 molecules were equally susceptible to clearance by Msp1. By contrast, we found evidence for a temporal maturation process at peroxisomes that converts newly-resident Pex15 molecules from an Msp1-sensitive to an Msp1-resistant state. This conclusion received independent support from lifetime analysis of Pex15 molecules tagged with a tandem fluorescent timer. To define the molecular basis for these observations, we hypothesized that the Msp1-resistant state is enabled by Pex15's native interactions with other peroxisomal proteins. Indeed, co-immunoprecipitation analysis showed that the transmembrane protein Pex3 is a Pex15 binding partner, while acute degradation of Pex3 from peroxisomes *in situ* induced rapid Msp1-dependent turnover of peroxisomal Pex15. Our findings provide a working mechanistic model for how native Pex15 avoids Msp1 surveillance that can be generalized to native mitochondrial TA proteins. This work also validates a new microscopy toolkit applicable to mechanistic dissections of other quality control systems *in vivo*.

RESULTS

Efficient clearance of a full-integrated substrate from mitochondria by *de novo* Msp1 induction.

To generate a defined Msp1 substrate population prior to initiation of Msp1 activity, we devised a synthetic gene system for orthogonal drug-controlled expression of Pex15 and Msp1. Briefly, we created a yeast strain genetic background with two transcriptional activator-promoter pairs: 1. the doxycycline (DOX)-activated reverse tetracycline trans-activator (rTA) (Roney et al., 2016) for controlling expression of fluorescently-labeled Pex15 (YFP-Pex15) from the *TET* promoter; and 2. the β-estradiol-activated synthetic transcription factor Z4EV (McIsaac et al., 2013) for controlling Msp1 expression from the Z4EV-driven (*ZD)* promoter (Figure 1-Figure Supplement 1A-C). Next, we pre-loaded mitochondria with Pex15 in the absence of any detectable Msp1 (Figure 1-Figure Supplement 1A) by growing cells for 2 hours in the presence of a high DOX concentration (50 μg/ml) necessary to induce sufficient mitochondrial mistargeting (Figure 1A and see below). This was followed by 2 hours of DOX wash-out to allow for mitochondrial maturation of newly-synthesized YFP-Pex15 (Figure 1A). Using confocal microscopy, we could resolve the relatively faint mitochondrial YFP fluorescence from the much brighter punctate YFP fluorescence (corresponding to peroxisomes, see below) by signal co-localization with Tom70-mTurquoise2 (a mitochondrial marker; Figure 1B) (see Figure 1-Figure Supplement 2, Videos 1 and 2, and Experimental Methods for computational image analysis details). Lastly, we monitored changes in mitochondrial YFP-Pex15 fluorescence density by timelapse live-cell imaging in the presence or absence of β-estradiol to define the effect of *de novo* induction of Msp1 activity (Figure 1A). Starting with the same pre-existing mitochondrial Pex15 population, we found that *de novo* Msp1 induction significantly enhanced mitochondrial YFP signal decay (Figure 1B-C and Figure 1-

Figure Supplement 1D). We reached a similar conclusion when we used a deletion variant of Pex15 ($Pex15_{\Delta C30}$) that is efficiently mistargeted to mitochondria because it lacks a C-terminal peroxisome targeting signal (Okreglak and Walter, 2014)(Figure 2A-C and Figure 2-Figure Supplement 1). To establish if $Pex15_{\Delta C30}$ has become fully membrane-integrated prior to Msp1 induction, we harvested cells after DOX treatment. Following cell lysis, we isolated crude mitochondria by centrifugation and treated them with Proteinase K (PK). Immunoblotting analysis against a C-terminal epitope engineered on Pex15 revealed the existence of a protected TMS-containing fragment that became PK-sensitive after solubilizing mitochondrial membranes with detergent (Figure 2D). Taken together, these findings argue that Msp1 can extract a fully-integrated substrate from the mitochondrial outer membrane and gave us a new tool for mechanistic dissection of Msp1 function *in vivo*.

Differential kinetic signatures of mitochondrial versus peroxisomal Pex15 clearance by Msp1

While performing the previous analysis, we observed that β-estradiol also enhanced YFP-Pex15 signal decay at punctate, non-mitochondrial structures. To test if these punctae corresponded to peroxisomes, we used a strain with mCherry-marked peroxisomes (mCherry-PTS1) and induced YFP-Pex15 expression with a lower DOX concentration (10 μg/ml). Indeed, we saw robust YFP and mCherry signal co-localization with little apparent Pex15 mistargeting to mitochondria (Figure 3A-B). As we initially surmised, β-estradiol-driven Msp1 expression enhanced YFP-Pex15 signal decay at peroxisomes (Figure 3A-C and Figure 3-Figure Supplement 1A). Western blotting analysis of lysates prepared from comparably-treated cells provided further support for our conclusion that *de novo* induction of Msp1 activity enables degradation of peroxisomal Pex15 (Figure 3D). Notably, Western blotting of lysates did not show the same degree of YFP-Pex15

turnover in the absence of Msp1 induction as was observed in cell microscopy. We harvested equal volumes of a dividing cell culture for each Western blotting timepoint whereas our cell microscopy monitors levels of YFP-Pex15 in individual organelles, and therefore YFP-Pex15 dilution through peroxisome fission and cell division may explain this discrepancy.

To our knowledge, Msp1-induced turnover of peroxisomal Pex15 had not been reported previously. We found two pieces of evidence that this unexpected phenotype was the product of Pex15 overexpression. First, treatment of *pTET-YFP-PEX15* cells with the lower (10 μg/ml) DOX concentration still induced a >10-fold higher YFP fluorescence at peroxisomes relative YFP-Pex15 expressed from its native promoter (Figure 3-Figure Supplement 1B-C). Second, we could detect no difference in natively-expressed peroxisomal Pex15 levels when we compared wild-type and *msp1Δ* cells (Figure 3E). This is unlikely a signal detection problem because we could robustly detect the accumulation of natively-expressed $Pex15_{\Delta C30}$ at mitochondria in *msp1Δ* cells (Figure 3E).

Why does Msp1-dependent turnover of peroxisomal Pex15 necessitate excess substrate when the same AAA machine clears mitochondria of even trace amounts of mistargeted Pex15? In search of an answer to this question, we repeated our analysis at higher temporal resolution and found a major difference between the kinetic signatures of mitochondrial and peroxisomal Pex15 turnover by Msp1 (Figure 4A and see below). Specifically, while mitochondrial Pex15 turnover showed simple exponential decay (*i.e.* linear decay after log-transformation), the decay of peroxisomal Pex15 appeared to be more complex, comprising faster and slower kinetic components. We detected no major kinetic differences between Msp1 targeting to mitochondria

and peroxisomes that could explain this phenomenon (Figure 1-Figure supplement 1B-C) but found a potential clue from a proteome-wide pulse-chase study showing that while most proteins decay exponentially, some exhibit non-exponential decay that can be explained by their stoichiometric excess over their binding partners (McShane et al., 2016). Since peroxisomal membranes have unique residents that interact with native Pex15, we hypothesized that non-exponential decay of overexpressed peroxisomal Pex15 arises due to the existence of an Msp1-sensitive "solitary" Pex15 state and an Msp1-insensitive "partner-bound" Pex15 state. This solitary state would be minimally populated by endogenously expressed Pex15 under steady-state conditions, but a significant fraction of overexpressed Pex15 molecules would be solitary because of stoichiometric excess. By contrast, since mitochondria are unlikely to have Pex15-binding partners, mitochondrial Pex15 would exist in an obligate solitary state and would therefore decay exponentially.

To test this hypothesis, we fit our microscopic YFP-Pex15 decay data against two competing stochastic models, which were previously used to describe proteome-wide protein decay data (see Experimental Methods for modelling details)(McShane et al., 2016). In the 1-state (exponential) model (Figure 4B, left), we posit that all Pex15 molecules have the same probability of decay (k_{decay}). In the 2-state (non-exponential) model (Figure 4B, right), we introduce the probability (k_{mat}) of nascent Pex15 maturation, alongside distinct probabilities for decay of the nascent ($k_{decay,1}$) and mature ($k_{decay,2}$) Pex15 states. Because the 2-state model contains two additional parameters, it is more susceptible to overfitting than the 1-state model. To avoid this problem, we compared our fits using the Akaike Information Criterion (see Experimental Methods), which provides a parameter-adjusted assessment of fit quality.

To analyze mitochondrial Msp1 substrate turnover, we chose YFP-Pex15$_{\Delta C30}$ over wild-type Pex15 to avoid measuring weak mitochondrial signals juxtaposed to strong peroxisomal signals. We also restricted our analysis to the first 60 minutes of β-estradiol treatment because longer Msp1 induction times led to a significant fraction of mitochondria with no detectable YFP signal, which would interfere with turnover fitting (Figure 4-Figure Supplement 1A). From this analysis, we concluded that the 1-state model was the better fit in both the presence and absence of Msp1 and that the effect of Msp1 was to increase the overall rate of signal decay (Figure 4C-D and Figure 4-Figure Supplement 1C). Turning to overexpressed YFP-Pex15 at peroxisomes, we found that the 1-state model was a better fit for Pex15 turnover in the absence of Msp1, which could be explained by simple signal dilution due to exponential cell division. In contrast, the 2-state model provided a much better explanation for signal decay in the presence of Msp1 (Figure 4E-F and Figure 4-Figure Supplement 1B-C). The effect became more pronounced when comparing fits that included later timepoints (Figure 4F, inset). From the parameter analysis of the best fits, we found that Pex15 in the nascent state decayed >4-fold faster ($k_{decay,\ 1} = 2.86\ hr^{-1}$) than Pex15 in the mature state ($k_{decay,\ 2} = 1.09\ hr^{-1}$).

Msp1 selectively clears newly-resident Pex15 molecules from peroxisomes

The 1-state and 2-state models of peroxisomal Pex15 turnover make distinct predictions about the effect of Msp1 expression on the age of Pex15 molecules. Specifically, in the 1-state model, transient Msp1 overexpression in cells with constitutive Pex15 expression should equally destabilize all Pex15 molecules, thus rapidly reducing their mean age over time (Figure 5B, top left panel). By contrast, in the 2-state model, Pex15 age should be buffered against Msp1

overexpression because of two opposing forces (Figure 4B and Figure 5B, top right panel): At one end, there would be an increase in $k_{decay,1}$ leading to less nascent Pex15, which would drive down the mean age over time. However, there would also be an opposing consequence of rapid depletion of new peroxisomal Pex15 by Msp1: the mature population of Pex15 would receive fewer (younger) molecules, which would drive up the mean age over time. Notably, both models predict that transient Msp1 expression would result in a decrease in peroxisomal Pex15 levels, albeit with differing kinetics (Figure 5B, bottom panels). We simulated Pex15 levels and age following transient Msp1 activation in the 1- and 2-state models with a set of possible half-lives that ranged from our microscopically determined value of 58 minutes to as slow as 143 minutes, as reported in the literature (Belle et al., 2006) (Figure 5B). Since our half-life value includes decay due to dilution from cell division, it is likely an underestimate of the actual value.

To measure the effect of Msp1 overexpression on the age of Pex15 molecules, we N-terminally tagged natively-expressed Pex15 with a tandem fluorescent timer (tFT-Pex15) (Figure 5-Figure Supplement 1A and Khmelinskii et al., 2012) comprising a slow-maturing mCherry and a rapidly-maturing superfolder YFP (sfYFP). On a population level, the mean ratio of mCherry to sfYFP fluorescence is a hyperbolic function of tFT-Pex15 age (Figure 5-Figure Supplement 1B and Khmelinskii et al., 2012). In this strain background, we marked peroxisomes using mTurquoise2-PTS1 and induced overexpression of Msp1 from a *ZD* promoter using β-estradiol (Figure 5A). Live-cell confocal microscopy combined with computational image analysis revealed a progressive reduction in peroxisomal sfYFP signal following Msp1 overexpression consistent with the predictions of both models, though with kinetics more akin to the predictions of the 2-state model (Figure 5B-C, bottom panels). More strikingly, the peroxisomal mCherry:sfYFP

fluorescence ratio was insensitive to β-estradiol treatment, consistent with the prediction of the 2-state model (Figure 5B-C, top panels). Collectively, our experimental evidence and theoretical analysis strongly support the existence of a Pex15 maturation process at peroxisomes that converts newly-synthesized Pex15 molecules from an Msp1-sensitive to an Msp1-insensitive state.

Pex3 is a Pex15-interacting protein that protects Pex15 from Msp1-dependent clearance at peroxisomes

To gain insight into the molecular basis of Pex15 maturation at peroxisomes, we hypothesized the existence of peroxisomal proteins that interact with Pex15 and whose absence would reveal that natively-expressed Pex15 is a latent substrate for Msp1. The cytosolic AAA proteins Pex1 and Pex6 are two prime candidates for testing this hypothesis because they form a ternary complex with Pex15 (Birschmann et al., 2003). However**,** we did not observe the expected decrease in YFP-Pex15 levels in *pex1Δ* or *pex6Δ* cells that would be indicative of enhanced turnover by Msp1 (Figure 6-Figure Supplement 1A). To look for additional Pex15 binding partners, we noted that the Pex1/6/15 complex is a regulator of peroxisome destruction by selective autophagy (Kamber et al., 2015; Nuttall et al., 2014). This process is initiated by Atg36, a receptor protein bound to the peroxisomal membrane protein Pex3 (Motley et al., 2012). Indeed, we found that Pex15 interacts with Pex3 by co-immunoprecipitation analysis (Figure 6-Figure Supplement 1B) . Before we could test if Pex3 protects Pex15 from Msp1-dependent turnover, we had to overcome a major technical challenge. Specifically, Pex3 is essential for targeting of numerous peroxisomal membrane proteins, which is why *pex3Δ* cells lack functional peroxisomes (Fang et al., 2004). Since Pex3 is normally turned over very slowly (Figure 6-Figure Supplement 1F and Belle et al., 2006), promoter shut-off is not a suitable method for acutely depleting Pex3. Instead, we developed

an auxin-inducible degradation system that rapidly eliminates Pex3 from peroxisomes *in situ.* First, we appended a tandem V5 epitope tag followed by an Auxin-inducible degron sequence (Nishimura et al., 2009) to the cytosolic C-terminus of Pex3 (Pex3-V5-AID). Next, we overexpressed an E3 ubiquitin ligase from rice (OsTir1) that binds and ubiquitinates the AID to enable degradation of AID fusions by the proteasome. OsTir1 overexpression can by itself stimulate basal protein turnover of AID fusions, but degradation is potentiated by Auxin addition. Indeed, Western blotting analysis for the V5 epitope revealed that Auxin addition induced rapid Pex3 destruction, which was dependent on OsTir1 expression and independent of Msp1 (Figure 6-Figure Supplement 1D-G). Importantly, microscopic analysis of cells co-expressing Pex3-GFP-AID and mCherry-PTS1 revealed that peroxisomes persisted for hours following Pex3 destruction (Figure 6-Figure Supplement 1D).

Having established a system for acute destruction of Pex3*,* we introduced it into either wild-type or *msp1Δ* genetic backgrounds containing doxycycline-inducible YFP-Pex15. After pre-loading peroxisomes with YFP-Pex15, we treated cells with Auxin and used live-cell confocal microscopy combined with computational image analysis to monitor changes in peroxisomal YFP fluorescence density for 2 hours (Figure 6A-B and Figure 6-Figure Supplement 1C). Strikingly, we observed that Auxin treatment immediately increased the rate of Msp1-dependent Pex15 turnover (Figure 6B). Thus, acute removal of the Pex15-interacting protein Pex3 from peroxisomes *in situ* unmasks Pex15 as a latent substrate for Msp1-dependent destruction.

DISCUSSION

Errors in TA protein targeting by the GET pathway pose a constant threat to mitochondrial health. Two recent studies revealed that yeast Msp1 (ATAD1 in humans), a AAA membrane protein resident on the surface of mitochondria and peroxisomes, is part of a conserved mechanism for preventing mistargeted TA proteins from accumulating in mitochondria (Chen et al., 2014b; Okreglak and Walter, 2014). At the same time, this pioneering work raised an important question about Msp1's substrate selectivity: What distinguishes TA proteins mistargeted to mitochondria from TA proteins native to mitochondria and peroxisomes?

Here, we answer this question as it pertains to Pex15, a native peroxisomal TA protein known to be an Msp1 substrate when mistargeted to mitochondria. As our starting point, we used a new microscopy methodology to show that *de novo* induction of Msp1 activity clears a fully-integrated Pex15 variant from mitochondria (Figure 7). This result solidifies the working model in the literature that Msp1 is a mechanoenzyme capable of extracting its substrates from the membrane and should encourage biochemical reconstitution of Msp1's function using liposomes with fully-integrated TA proteins. We were also able to reveal that peroxisomal Pex15 is a latent Msp1 substrate at peroxisomes. The key starting observation that led us to this conclusion was that Pex15 overexpressed at peroxisomes was turned over by an unusual non-exponential process, which depended on Msp1 induction. By model fitting of these data and comparative analysis with the exponential decay of mitochondrial Pex15, we found evidence for a Pex15 maturation mechanism unique to peroxisomes. By positing that this mechanism converts newly-resident peroxisomal Pex15 from an initial Msp1-sensitive state to an Msp1-resistant state, we were able to account for the non-exponential decay kinetics (Figure 7). Moreover, we validated a key

prediction of this mechanism by showing that Msp1 selectively removes peroxisomal Pex15 from the young end of the age distribution.

The molecular details that enable Pex15 maturation into an Msp1-resistant state remain to be worked out. However, our evidence strongly argues that peroxisomal membrane protein Pex3 is a critical component of this process. Pex3 has been previously shown to play a role in the insertion of peroxisomal membrane proteins (Fang et al., 2004). Thus, it is possible that loss of Pex3 function leads to indirect loss of another membrane protein that itself blocks Msp1-dependent turnover of Pex15. We cannot formally exclude this possibility but we find it unlikely for two reasons. First, we showed that Pex3 co-immunoprecipitates with Pex15. Thus, in principle, Pex3 is well-positioned to either occlude an Msp1 binding site on Pex15 or make Pex15 structurally more resistant to mechanodisruption. Second, our engineered Pex3 degradation system is very rapid and its activation causes a near-instantaneous increase in Msp1-dependent Pex15 turnover rate. Thus, for this to be an indirect effect, it would have to be mediated by a membrane protein whose basal turnover was comparably fast. Settling this issue is an important future goal that will be facilitated by assaying Msp1 function with purified components. More broadly, a simple extension of our working model for Msp1 substrate selectivity leads to the intriguing hypothesis that native mitochondrial TA proteins are shielded from Msp1 by their binding partners. The new microscopy methodology we have described here will facilitate testing of this idea in the near future.

It is useful to compare the function of Msp1 with that of FtsH, its closest relative in *Escherichia coli*. This AAA protease is known to destroy excess copies of membrane-integral components of

several complexes, including the bacterial Sec translocon (Kihara et al., 1995; Westphal et al., 2012). The topological diversity of FtsH substrates argues that they are selected as substrates by exposing generic degron features such as hydrophobic patches or locally unstructured regions in their uncomplexed states. Thus far, only TA proteins have been defined as *bona fide* Msp1 substrates but we speculate that Msp1, analogous to FtsH, can also recognize other membrane proteins that exist in a solitary state for prolonged periods of time. In this light, it will be interesting to test if the human Msp1 homolog ATAD1 protects mitochondria from accumulating peroxisomal membrane proteins in certain Zellweger Spectrum disorders (Muntau et al., 2000).

Lastly, our work provides a broad perspective for seeing the role of Msp1 as a quality control factor. All quality control mechanisms face the challenge of substrate conditionality: a non-substrate at one location or point in time can become a substrate at another. For certain ER-associated degradation (ERAD) mechanisms this challenge comes in the form of distinguishing recently translocated glycoproteins in the ER (an unfolded species) from glycoproteins that have failed to fold in the ER despite prolonged residence (reviewed in Shao and Hegde, 2016). To achieve accurate substrate selection, specific ERAD factors query the age of unfolded proteins for the presence of glycans that have become trimmed with time to serve as degradation signals (Clerc et al., 2009; Quan et al., 2008). Interestingly, the glycosidase responsible for glycan trimming must be under tight expression control because its overexpression results in premature destruction of nascent glycoprotein (Wu et al., 2003). By comparison, we have shown that overproduction of Msp1 inappropriately destabilizes nascent peroxisomal Pex15 molecules, presumably by outpacing their normal maturation into an Msp1-resistant state. Consequently, peroxisomes overexpressing Msp1 eventually lose competency for matrix protein import (data not shown), a

process that depends on Pex15 (Matsumoto et al., 2003). Thus, our work reveals how diverse quality control mechanisms set time delays for substrate selection to balance tight surveillance against hypervigilant destruction.

Experimental methods

Yeast strain construction

All *S. cerevisiae* strains were constructed using standard homologous recombination methods (Longtine et al., 1998) and are listed in the strain table. Cassettes for fluorescent protein tagging at genes' endogenous loci were generated by PCR amplification from the pKT vector series (Sheff and Thorn, 2004). Tandem fluorescent timer-tagged *PEX15* strains were made by integrating a PCR product consisting of the *PEX15* promoter, an *sfYFP* gene with no stop codon, an *mCHERRY* gene with no stop codon, and the *PEX15* coding sequence and terminator followed by a geneticin resistance cassette into the *URA3* locus of the parent strain. $pex15_{\Delta C30}$ was generated by sewing PCR. Fluorescent peroxisome markers were generated by creating pKT plasmid variants containing the *S. cerevisiae TDH3* promoter upstream of the fluorescent protein gene and a PTS1 sequence (Serine-Lysine-Leucine) before the fluorescent protein's stop codon. This fragment along with the marker cassette contained within the plasmid was integrated into strains' *TRP1* locus. For integration of the *Z4EV* transcription factor gene-*ZD* promoter cassette (McIsaac et al., 2013) upstream of *MSP1*, a PCR product containing a *LEU* marker, the *Z4EV* transcription factor cassette, and a *GAL1* promoter variant altered for control by Z4EV was integrated immediately 5' to the *MSP1* coding sequence. For doxycycline-induced expression of *PEX15* variants, a similar PCR product was generated consisting of a *TRP* marker cassette, the G72V variant of the reverse tetracycline transactivator (*rTA*) (Roney et al., 2016), a *GAL1* promoter variant altered for control by rTA, the *YFP* gene with no stop codon, the *PEX15* gene or mutant variant, and the *PEX15* terminator. This cassette was integrated into the strain's *URA3* locus. *PEX3-FLAG* was generated by integrating a 3×FLAG tag sequence, *CYC1* terminator, and a nourseothricin resistance cassette before the native PEX3 stop codon.

Whole cell lysate immunoblotting

Lysate preparation

Yeast cultures were grown overnight to mid-exponential phase at 30 °C in YEPD (1% yeast extract, 2% bacto-peptone, 2% glucose) and treated with 3-indoleacetic acid (auxin, 500 μM) (Sigma), cycloheximide (100 μg/mL) (Sigma) or DMSO vehicle as indicated. Cells were pelleted by 3000×g centrifugation for 1 minute, resuspended in ice cold 0.2 M NaOH and incubated on ice for 10 minutes. Cells were pelleted by 10,000×g centrifugation for 1 minute and then resuspended and boiled in SDS-PAGE sample buffer (50 mM Tris-HCl pH 6.8, 2.5% sodium dodecyl sulfate, 0.008% bromophenol blue, 10% glycerol, 5% β-mercaptoethanol). Cell debris was pelleted and supernatants were used for SDS-PAGE and Western blotting analysis.

Immunoblotting

Samples were run on Novex 4-20% Tris-Glycine gels (Life Technologies) for 70 minutes at 195V, then transferred to nitrocellulose membranes and blotted using standard protocols. Blocking and antibody incubations were performed in 5% milk in TBST (10 mM Tris-HCl pH 7.4, 150 mM NaCl, 0.25 mM EDTA, 0.05% Tween-20). HRP-conjugated secondary antibodies were detected using SuperSignal West Femto Substrate (Thermo Scientific) on a ChemImager (AlphaInnotech) or fluorescent secondary antibodies were detected using a Typhoon Trio imager (GE Healthcare).

Protease protection of YFP-Pex15$_{\Delta C30}$-V5 at mitochondria

Yeast culture

pTET-YFP-PEX15ΔC30-V5 cells were pre-grown to mid-log phase (OD600 = 1) in 100 mL YEPD and then diluted to OD600 = 0.1 in 1 L YEPD. Cells were grown with shaking at 30 °C to an OD600 of 1 and then treated with 50 μg/ml doxycycline (Sigma) for 4 hours at 30 °C with shaking. Cells were harvested by centrifugation.

Mitochondria isolation

Crude mitochondria were isolated as described previously (Meisinger et al., 2006).

Protease protection

100 μg of crude mitochondria were subjected to treatment with 5 μg Proteinase K (Roche) or mock treatment in the presence or absence of 1% Triton X-100 (Sigma) on ice for 60 minutes. Phenylmethanesulfonyl fluoride (PMSF) (Sigma) was added to each sample to a final concentration of 2 mM to inhibit Proteinase K and samples were incubated 10 minutes on ice. Samples were mixed with boiling SDS-PAGE sample buffer and subjected to SDS-PAGE and immunoblotting analysis as described earlier.

Live-cell imaging of tagged Pex15 and Msp1

Yeast culture

Cells were inoculated into 2 mL complete synthetic media with glucose (0.67% yeast nitrogen base, 2% glucose, 1×CSM (Sunrise Sciences)) and grown overnight at 30 °C on a roller drum. The following morning, cells were back-diluted to a cell density of 0.05 OD_{600} units/mL in fresh media and grown to mid-log phase (density 0.5-1 OD_{600} units/mL) for imaging, with drug treatments as indicated in experiment schematics. β-estradiol (Sigma) was used at 1 μM for all experiments;

doxycycline was used at concentrations indicated in figure legends. Cells in culture media were applied directly to the well of a concanavalin A (MP Biomedicals)-coated Lab-Tek II chambered coverglass (Thermo Fisher) and incubated 5 minutes at room temperature to adhere. Culture media was removed and adhered cells were immediately overlaid with a 1% agarose pad containing complete synthetic media with glucose and supplemented with drugs when applicable. The agarose pad was overlaid with liquid media for timelapse imaging experiments.

Confocal fluorescence microscopy

Live-cell imaging was performed at 25 °C on a TI microscope (Nikon) equipped with a CSU-10 spinning disk (Yokogawa), an ImagEM EM-CCD camera (Hamamatsu), and a 100× 1.45 NA objective (Nikon). The microscope was equipped with 447 nm, 515 nm and 591 nm wavelength lasers (Spectral) and was controlled with MetaMorph imaging software (Molecular Devices). Z-stacks were acquired with 0.2 µm step size for 6 µm per stack. Camera background noise was measured with each Z-stack for normalization during timelapse imaging.

Sample size estimation and experimental replication details

For quantitative microscopy experiments, the number of cells present in each sample was manually counted in brightfield images and indicated in the associated figure legend. Each experiment was repeated as indicated in the associated figure legend. Replicates represent technical replicates in which the same strains were subjected to repeats of the entire experiment, often on different days.

Image post-processing and organelle segmentation

First, all fluorescence images were normalized to background noise to compensate for uneven illumination and variability in camera background signal. To identify peroxisomes and mitochondria, organelle marker images were processed by an object segmentation script. Briefly, images were smoothed using a Gaussian filter and then organelle edges were identified by processing each slice with a Canny edge detector (Canny, 1986) implemented in the Python package scikit-image. Enclosed objects were filled and individual three-dimensional objects were identified by locally maximizing Euclidean distance to the object border. Individual objects were identified and separated by watershed segmentation as implemented in scikit-image. For mitochondria, contiguous but separately segmented objects were merged to form one mitochondrion. For YFP-Pex15 quantitation at mitochondria, regions of mitochondria that overlapped with peroxisomes were removed by eliminating mitochondrial pixels that overlapped with segmented peroxisomes. Segmentation code is available at www.github.com/denic_lab/pyto_segmenter and sample implementation is available at www.github.com/denic_lab/Weir_2017_analysis. Raw source images are available on the Dryad data repository associated with this manuscript.

Fluorescence intensity analysis

Following organelle segmentation, total fluorescence intensity for Pex15 was determined in each segmented object by summing intensities in the corresponding pixels for YFP fluorescence images (and mCherry images for mCherry-sfYFP-Pex15 and mCherry-sfYFP-Pex15$_{\Delta C30}$ in Figure 3). Fluorescence density was calculated by dividing total pixel intensity by object volume in pixels. Background was calculated empirically by measuring Pex15 fluorescence intensity in peroxisomes and/or mitochondria in cells lacking fluorescently labeled Pex15, and the mean background density

was subtracted from each segmented object's fluorescence density. Because Pex15 fluorescence density was roughly log-normally distributed, mean and standard error of the mean were calculated on logarithmically transformed fluorescence densities when applicable. Plotting was performed using R and the ggplot2 package. See www.github.com/denic_lab/Weir_2017_analysis for tabulated data and analysis code.

Model fitting and statistics

For 1-state and 2-state model fitting, organelle fluorescence density means were first normalized to the sample's mean at time 0. For the 1-state model, log-transformed mean fluorescence densities at each time point were fit to a linear model using least squares fitting in R. Peroxisome size decreased in some cells over the course of the timelapse imaging described in Figure 4E-F, resulting in size-dependent artefactual changes in measured YFP fluorescence density at peroxisomes. We therefore exclusively analyzed larger peroxisomes (volume > 150 pixels, which corresponded to the size of the starting population) to accurately monitor changes in YFP fluorescence density throughout the timecourse. For the 2-state model, logarithmically transformed data was fit to a logarithmically transformed version of a previously derived 2-state degradation model (Sin et al., 2016) using non-linear least squares fitting in R. The better model fit was determined using the Akaike Information Criterion adjusted for small sample size, and p-values for model preference were calculated as described previously (McShane et al., 2016). Observed half-life was determined by converting the peroxisomal YFP-Pex15 –Msp1 k_{decay} (Figure 4-Figure Supplement 1C) using the equation half-life = $\ln(2)/k_{decay}$, and then multiplied by 60 to convert from hours to minutes.

As indicated by figure legends, error bars represent standard error of the mean when present.

Simulation of protein age and turnover

To stochastically model peroxisomal Pex15 levels and age following transient *MSP1* expression we used a Gillespie algorithm approach (Gillespie, 1977). In brief, this approach cycles through the following steps: 1. Model the expected time until the next "event" takes place (import, degradation, or maturation of a Pex15 molecule) by summing event rates and drawing from an exponential distribution based on the summed rate constant, 2. Age all simulated Pex15 molecules according to time passage, 3. Determine which of the possible events took place by weighted random draws based on each event's probability of occurring, 4. Execute that event, and then repeat these steps until the simulation's time has expired. Based on our observation that Pex15 turnover in the absence of Msp1 occurs with exponential decay kinetics (Figure 4F), we established starting conditions by drawing 1000 ages from an exponential distribution with half-life indicated in Figure 5B. For the rest of the simulation we used this rate constant to predict import of new molecules and as a steady-state degradation rate constant (and as $k_{decay,2}$ in 2-state simulations). We treated this vector of 1000 ages as a single peroxisome containing 1000 Pex15 molecules (this is likely an over-estimation of Pex15 amounts in many cases, but over-estimating Pex15 levels improved statistical robustness of the analysis and did not alter simulation mean outcomes). When simulating steady state 2-state behavior using the calculated k_{mat} value, we found that ~60% of the elements existed in the "unstable" form at steady state (data not shown) and therefore used this as a starting value. For 2-state simulations we randomly drew 600 of the vector elements to be "unstable" at the start of the simulation, weighting probabilities of each draw using an exponential distribution with k_{mat} as the decay rate constant. After validating that our starting conditions

represented a stable steady state by simulating without perturbing rate constants, we began the reported simulations with k_{decay} set to 2.38 hr^{-1}, the best linear fit for turnover from the first 4 time points (for 1-state simulations), or with $k_{decay,1}$ (for 2-state simulations) set to the calculated value from Figure 4F. Simulations ran for 4 hours of simulated time and values for particle age and abundance were recorded at every simulated minute. 100 simulations were performed with each set of parameters and the mean particle age and abundance at each minute were calculated across the 100 simulations. Finally, we modeled maturation of sfYFP fluorescence and mCherry fluorescence based on established maturation half-times (Hansen and O'Shea, 2013; Khmelinskii et al., 2012, respectively) and calculated the mean population tFT ratio at each minute. We normalized these data to the value at the simulation's starting point. See the Denic Lab Github repository for this paper for analysis code details.

Pex3-GFP-AID fluorescence microscopy

Yeast cultures were grown overnight in synthetic medium to logarithmic phase, treated with 3-indoleacetic acid (Auxin, 1 mM) (Sigma) or DMSO vehicle as indicated, concentrated, and imaged at room temperature on an Axiovert 200M microscope body (Carl Zeiss) equipped with a CSU-10 spinning disk (Yokogawa) and 488 nm and 561 nm lasers (Coherent), using an oil-immersion 100× 1.45 NA objective (Carl Zeiss). Images were acquired using a Cascade 512B EM-CCD detector (Photometrics) and MetaMorph acquisition software (Molecular Devices).

Pex3-FLAG immunoprecipitation

Culture growth and cell lysis

2 L yeast cells were grown to OD_{600} = 1.6-2.0 in YEP + 5% glucose at 30 °C with shaking. Cells were collected by centrifuging 5 minutes at 3000×g, 4 °C, then washed once with 50 ml sterile H_2O. Cells were resuspended in 2 ml ice-cold lysis buffer (50 mM HEPES-KOH pH 6.8, 150 mM KOAc, 2 mM $MgCl_2$, 1 mM $CaCl_2$, 0.2 M sorbitol, cOmplete protease inhibitor tablet (Sigma), 1 mM phenylmethylsulfonylfluoride (Sigma)) and dripped into liquid nitrogen to flash-freeze. Cells were lysed cryogenically using a PM100 ball mill (Retsch) and stored at -80 °C.

Lysate preparation and immunoprecipitation

2 g lysed cell powder was thawed on ice and mixed with 4 mL IP buffer (50 mM HEPES-KOH pH 6.8, 150 mM KOAc, 2 mM $Mg[Oac]_2$, 1 mM $CaCl_2$, 15% glycerol, 1% NP-40). Lysates were nutated 1 hour at 4 °C, centrifuged twice at 3000 rpm, 4 °C for 5 minutes to remove unlysed cells, and then supernatants were subjected to a 30 minute, 100,000×g ultracentrifugation step. Ultracentrifugation supernatants (inputs) were mixed with 20 µL protein G Dynabeads (Sigma) conjugated to anti-FLAG M2 monoclonal antibody (Sigma) and nutated 3 hours at 4 °C. Dynabeads were washed 4 times with IP buffer and bound proteins were eluted with 20 µl 1 mg/mL 3×FLAG peptide (Sigma) in IP buffer. Immunoblotting analysis was performed as described above.

AUTHOR CONTRIBUTIONS: N.R.W. performed most of the experiments described in this study and analyzed the data. R.A.K. performed Pex3 immunoprecipitations. J.S.M. established the Pex3-AID system and performed control experiments. N.R.W., J.S.M., and V.D. examined the data. V.D. conceived the project, guided the experiments, and wrote the paper with N.R.W. and input from J.S.M. and R.A.K.

ACKNOWLEDGEMENTS: We thank A. Murray, E. O'Shea, D. Botstein, N. Pfanner, and A. Amon for reagents, S. Mukherji for modeling advice, L. Bagamery for microscopy assistance, and members of the Denic Laboratory, M. Gropp, A. Murray, and R. Gaudet for comments on the manuscript. This work was supported by the National Institutes of Health (R01GM099943-04).

REFERENCES

Belle, A., Tanay, A., Bitincka, L., Shamir, R., and O'Shea, E.K. (2006). Quantification of protein half-lives in the budding yeast proteome. Proc. Natl. Acad. Sci. *103*, 13004–13009.

Birschmann, I., Stroobants, A.K., Berg, M. van den, Schäfer, A., Rosenkranz, K., Kunau, W.-H., and Tabak, H.F. (2003). Pex15p of Saccharomyces cerevisiae Provides a Molecular Basis for Recruitment of the AAA Peroxin Pex6p to Peroxisomal Membranes. Mol. Biol. Cell *14*, 2226–2236.

Borgese, N., and Fasana, E. (2011). Targeting pathways of C-tail-anchored proteins. Biochim. Biophys. Acta BBA - Biomembr. *1808*, 937–946.

Canny, J. (1986). A Computational Approach to Edge Detection. IEEE Trans Pattern Anal Mach Intell *8*, 679–698.

Chen, Y., Pieuchot, L., Loh, R.A., Yang, J., Kari, T.M.A., Wong, J.Y., and Jedd, G. (2014a). Hydrophobic handoff for direct delivery of peroxisome tail-anchored proteins. Nat. Commun. *5*, 5790.

Chen, Y.-C., Umanah, G.K.E., Dephoure, N., Andrabi, S.A., Gygi, S.P., Dawson, T.M., Dawson, V.L., and Rutter, J. (2014b). Msp1/ATAD1 maintains mitochondrial function by facilitating the degradation of mislocalized tail-anchored proteins. EMBO J. *33*, 1548–1564.

Clerc, S., Hirsch, C., Oggier, D.M., Deprez, P., Jakob, C., Sommer, T., and Aebi, M. (2009). Htm1 protein generates the N-glycan signal for glycoprotein degradation in the endoplasmic reticulum. J. Cell Biol. *184*, 159–172.

Denic, V., Dötsch, V., and Sinning, I. (2013). Endoplasmic Reticulum Targeting and Insertion of Tail-Anchored Membrane Proteins by the GET Pathway. Cold Spring Harb. Perspect. Biol. *5*, a013334.

Fang, Y., Morrell, J.C., Jones, J.M., and Gould, S.J. (2004). PEX3 functions as a PEX19 docking factor in the import of class I peroxisomal membrane proteins. J Cell Biol *164*, 863–875.

Gillespie, D.T. (1977). Exact stochastic simulation of coupled chemical reactions. J. Phys. Chem. *81*, 2340–2361.

Hansen, A.S., and O'Shea, E.K. (2013). Promoter decoding of transcription factor dynamics involves a trade-off between noise and control of gene expression. Mol. Syst. Biol. *9*, 704.

Hegde, R.S., and Keenan, R.J. (2011). Tail-anchored membrane protein insertion into the endoplasmic reticulum. Nat. Rev. Mol. Cell Biol. *12*, 787–798.

Jonikas, M.C., Collins, S.R., Denic, V., Oh, E., Quan, E.M., Schmid, V., Weibezahn, J., Schwappach, B., Walter, P., Weissman, J.S., et al. (2009). Comprehensive characterization of genes required for protein folding in the endoplasmic reticulum. Science *323*, 1693–1697.

Kamber, R.A., Shoemaker, C.J., and Denic, V. (2015). Receptor-Bound Targets of Selective Autophagy Use a Scaffold Protein to Activate the Atg1 Kinase. Mol. Cell *59*, 372–381.

Khmelinskii, A., Keller, P.J., Bartosik, A., Meurer, M., Barry, J.D., Mardin, B.R., Kaufmann, A., Trautmann, S., Wachsmuth, M., Pereira, G., et al. (2012). Tandem fluorescent protein timers for in vivo analysis of protein dynamics. Nat. Biotechnol. *30*, 708–714.

Kihara, A., Akiyama, Y., and Ito, K. (1995). FtsH is required for proteolytic elimination of uncomplexed forms of SecY, an essential protein translocase subunit. Proc. Natl. Acad. Sci. U. S. A. *92*, 4532–4536.

Longtine, M.S., Mckenzie III, A., Demarini, D.J., Shah, N.G., Wach, A., Brachat, A., Philippsen, P., and Pringle, J.R. (1998). Additional modules for versatile and economical PCR-based gene deletion and modification in Saccharomyces cerevisiae. Yeast *14*, 953–961.

Matsumoto, N., Tamura, S., and Fujiki, Y. (2003). The pathogenic peroxin Pex26p recruits the Pex1p–Pex6p AAA ATPase complexes to peroxisomes. Nat. Cell Biol. *5*, 454–460.

McIsaac, R.S., Oakes, B.L., Wang, X., Dummit, K.A., Botstein, D., and Noyes, M.B. (2013). Synthetic gene expression perturbation systems with rapid, tunable, single-gene specificity in yeast. Nucleic Acids Res. *41*, e57–e57.

McShane, E., Sin, C., Zauber, H., Wells, J.N., Donnelly, N., Wang, X., Hou, J., Chen, W., Storchova, Z., Marsh, J.A., et al. (2016). Kinetic Analysis of Protein Stability Reveals Age-Dependent Degradation. Cell *167*, 803–815.e21.

Meisinger, C., Pfanner, N., and Truscott, K.N. (2006). Isolation of yeast mitochondria. Methods Mol. Biol. Clifton NJ *313*, 33–39.

Motley, A.M., Nuttall, J.M., and Hettema, E.H. (2012). Pex3-anchored Atg36 tags peroxisomes for degradation in Saccharomyces cerevisiae. EMBO J. *31*, 2852–2868.

Muntau, A.C., Mayerhofer, P.U., Paton, B.C., Kammerer, S., and Roscher, A.A. (2000). Defective Peroxisome Membrane Synthesis Due To Mutations in Human PEX3 Causes Zellweger Syndrome, Complementation Group G. Am. J. Hum. Genet. *67*, 967–975.

Nishimura, K., Fukagawa, T., Takisawa, H., Kakimoto, T., and Kanemaki, M. (2009). An auxin-based degron system for the rapid depletion of proteins in nonplant cells. Nat. Methods *6*, 917–922.

Nuttall, J.M., Motley, A.M., and Hettema, E.H. (2014). Deficiency of the exportomer components Pex1, Pex6, and Pex15 causes enhanced pexophagy in Saccharomyces cerevisiae. Autophagy *10*, 835–845.

Okreglak, V., and Walter, P. (2014). The conserved AAA-ATPase Msp1 confers organelle specificity to tail-anchored proteins. Proc. Natl. Acad. Sci. *111*, 8019–8024.

Olivares, A.O., Baker, T.A., and Sauer, R.T. (2016). Mechanistic insights into bacterial AAA+ proteases and protein-remodelling machines. Nat. Rev. Microbiol. *14*, 33–44.

Papić, D., Elbaz-Alon, Y., Koerdt, S.N., Leopold, K., Worm, D., Jung, M., Schuldiner, M., and Rapaport, D. (2013). The role of Djp1 in import of the mitochondrial protein Mim1 demonstrates specificity between a cochaperone and its substrate protein. Mol. Cell. Biol. *33*, 4083–4094.

Quan, E.M., Kamiya, Y., Kamiya, D., Denic, V., Weibezahn, J., Kato, K., and Weissman, J.S. (2008). Defining the glycan destruction signal for endoplasmic reticulum-associated degradation. Mol. Cell *32*, 870–877.

Roney, I.J., Rudner, A.D., Couture, J.-F., and Kærn, M. (2016). Improvement of the reverse tetracycline transactivator by single amino acid substitutions that reduce leaky target gene expression to undetectable levels. Sci. Rep. *6*, 27697.

Schuldiner, M., Metz, J., Schmid, V., Denic, V., Rakwalska, M., Schmitt, H.D., Schwappach, B., and Weissman, J.S. (2008). The GET Complex Mediates Insertion of Tail-Anchored Proteins into the ER Membrane. Cell *134*, 634–645.

Shao, S., and Hegde, R.S. (2016). Target Selection during Protein Quality Control. Trends Biochem. Sci. *41*, 124–137.

Sheff, M.A., and Thorn, K.S. (2004). Optimized cassettes for fluorescent protein tagging in Saccharomyces cerevisiae. Yeast *21*, 661–670.

Sin, C., Chiarugi, D., and Valleriani, A. (2016). Degradation Parameters from Pulse-Chase Experiments. PLOS ONE *11*, e0155028.

Westphal, K., Langklotz, S., Thomanek, N., and Narberhaus, F. (2012). A Trapping Approach Reveals Novel Substrates and Physiological Functions of the Essential Protease FtsH in Escherichia coli. J. Biol. Chem. *287*, 42962–42971.

Wu, Y., Swulius, M.T., Moremen, K.W., and Sifers, R.N. (2003). Elucidation of the molecular logic by which misfolded α1-antitrypsin is preferentially selected for degradation. Proc. Natl. Acad. Sci. *100*, 8229–8234.

FIGURE LEGENDS

Figure 1: Pulse-chase analysis of mitochondrial Pex15 turnover by Msp1.

A. Cells containing the doxycycline-inducible promoter driving YFP-Pex15 expression and the β-estradiol-inducible promoter driving Msp1 expression were grown for 2 hours in the presence of 50 μg/ml doxycycline (DOX) before they were washed and grown for 2 hours in drug-free media. Following this period of substrate pre-loading, half of the cells were exposed to 1 μM β-estradiol while the other half received vehicle, followed by time-lapse imaging of both cell populations using a spinning disk confocal microscope. This experiment was performed twice with similar results.

B. Representative confocal micrographs from the experiment described in part *A*. Each image represents a maximum intensity projection of a Z-stack. Red cell outlines originate from a single bright-field image acquired at the center of the Z-stack. Scale bar, 5 μm.

C. Quantitation of mitochondrial YFP-Pex15 fluorescence from the experiment described in part *A*. YFP-Pex15 fluorescence density corresponds to the total YFP-Pex15 signal at each computationally-defined mitochondrion (marked by Tom70-mTurquoise2) divided by the mitochondrial pixel volume (see Experimental Methods and Figure 1-Figure Supplement 2 for more details). Shown are violin plots of the resulting YFP-Pex15 density distributions. These data represent analysis of 150 mock-treated and 200 β-estradiol-treated cells followed throughout the time course as well as progeny from cell divisions during the experiment.

Figure 1-Figure Supplement 1: Supporting evidence for Msp1 turnover of YFP-Pex15 at mitochondria.

A. Quantitation of Msp1-YFP levels at mitochondria and peroxisomes in *pMSP1-MSP1-YFP* and un-induced *pZD-MSP1-YFP* cells. Msp1-YFP fluorescence density corresponds to the total Msp1-YFP signal at each computationally-defined mitochondrion marked by Tom70-mTurquoise2 (left) or peroxisome marked by mCherry-PTS1 (right) divided by the organelle's pixel volume (see Experimental Methods and Figure 1-Figure Supplement 2 for details). Shown are the mean fluorescence densities for each sample normalized to the *pMSP1*-driven Msp1-YFP mean fluorescence density at the same organelle. 0 is defined for each organelle as the mean YFP fluorescence density in untagged *MSP1* cells. Error bars represent standard error of the population mean. The *pZD-MSP1-YFP* data here are reproduced as the –β-estradiol 0 hour timepoint in part *C*.

B. Experimental timeline of the staged expression experiment for monitoring Msp1-YFP levels following *pZD* induction. Cells expressing Msp1-YFP from the *ZD* promoter at the native locus (the Z4EV expression cassette was integrated upstream of the *ZD* promoter) were pre-cultured before half of the cells were exposed to 1 μM β-estradiol while the other half received vehicle, followed by time-lapse imaging of both cell populations using a spinning disk confocal microscope.

C. Quantitation of mitochondrial (top) and peroxisomal (bottom) Msp1-YFP fluorescence density from the experiment described in part *B*. Msp1-YFP fluorescence density corresponds to the total Msp1-YFP signal at each computationally-defined mitochondrion marked by Tom70-mTurquoise2 (top) or peroxisome marked by mCherry-PTS1 (bottom) divided by the organelle's pixel volume (see Experimental Methods and Figure 1-Figure Supplement 2 for more details). Shown are the mean fluorescence densities for each sample

normalized to the *MSP1* promoter-driven Msp1-YFP mean at the same organelle. Error bars represent standard error of the population mean.

D. Quantitation of mitochondrial YFP-Pex15 fluorescence density from Figure 1C compared to autofluorescence background. Y axis represents the mitochondrial fluorescence density normalized to the mean autofluorescence in mitochondria segmented from cells lacking *TET-YFP-PEX15*, with 0 set to the minimum detected autofluorescence density at a mitochondrion. Shown are violin plots of the resulting YFP-Pex15 density distributions. Mitochondria were segmented from 129 cells lacking *TET-YFP-PEX15* to generate the autofluorescence distribution. Dashed line represents 3 standard deviations above the autofluorescence mean. In the *TET-YFP-PEX15*-containing cells analyzed here, 5 mitochondria out of 2284 (0.2%) displayed fluorescence densities below this 3 standard deviation cutoff. See Figure 1 for additional details.

Figure 1-Figure Supplement 2: Schematic of the processing pipeline for identifying mitochondria and peroxisomes from fluorescence microscopy images.

Beginning at the top left, fluorescence channels for mitochondria (cyan) and peroxisomes (magenta) are split into separate Z-stacks. After 3-dimensional Gaussian smoothing through the Z-stack, each individual slice is analyzed using a Canny edge detector (Canny, 1986) to identify object edges. Next, enclosed areas are filled to generate a mask representing areas of the slice containing mitochondria or peroxisomes. For mitochondria, holes in regions containing donut-shaped organelles are re-opened. Stacks are re-combined and a 3-dimensional Euclidean Distance Transformation is used to identify pixels within the masked organelles with the greatest distance to the edge of the object. These local

maxima are used as seed points for watershed-based object segmentation. For mitochondria, contiguous objects from watershedding are combined to form one mitochondrion. See Experimental Methods for additional details, and see Videos 1 and 2 for a comparison of fluorescent organelle marker image inputs to segmentation outputs.

Figure 2: Pulse-chase analysis of mitochondrial Pex15$_{\Delta C30}$ turnover by Msp1.

A. Experimental timeline of the staged expression experiment for monitoring Msp1-dependent turnover of mitochondrial YFP-Pex15$_{\Delta C30}$. 50 μg/ml DOX was used for induction. This experiment was performed twice with similar results.

B. Representative confocal micrographs from the experiment described in part *A*. Each image represents a maximum intensity projection of a Z-stack. Red cell outlines originate from a single bright-field image acquired at the center of the Z-stack. Scale bar, 5 μm.

C. Quantitation of mitochondrial YFP-Pex15$_{\Delta C30}$ fluorescence from the experiment described in part *B*. YFP-Pex15$_{\Delta C30}$ fluorescence density corresponds to the total YFP signal at each computationally-defined mitochondrion (marked by Tom70-mTurquoise2) divided by the mitochondrial pixel volume (see Experimental Methods for more details). These data represent analysis of 117 mock-treated and 132 β-estradiol-treated cells followed throughout the time course as well as progeny from cell divisions during the experiment. The 515 nm laser power was increased relative to the experiment in Figure 1 and therefore AUs are not comparable between these experiments.

D. Protease protection assay monitoring YFP-Pex15$_{\Delta C30}$-V5 integration into mitochondria. Crude mitochondria were isolated from *TET-YFP-pex15$_{\Delta C30}$-V5* cells (see Experimental Methods for details) and subjected to Proteinase K (PK) or mock treatment in the presence

or absence of 1% Triton X-100 (TX). Samples were resolved by SDS-PAGE and analyzed by immunoblotting with the indicated antibodies. Immunoblotting with an α-V5 antibody visualized bands at the predicted molecular weight for both full-length YFP-Pex15$_{\Delta C30}$-V5 (top) and a smaller protease-resistant fragment (bottom). The asterisk denotes a PK-resistant fragment that appears only in detergent-solubilized mitochondria. Immunoblotting was performed against the surface-exposed mitochondrial outer membrane protein Tom70 and the mitochondrial inner membrane protein Sdh4 to assess accessibility of different mitochondrial compartments to PK.

Figure 2-Figure Supplement 1: Supporting evidence for Msp1-dependent turnover of mitochondrial YFP-Pex15$_{\Delta C30}$.

Quantitation of mitochondrial YFP-Pex15$_{\Delta C30}$ fluorescence density from Figure 2C compared to autofluorescence background. Y axis represents the mitochondrial fluorescence density normalized to the mean autofluorescence in mitochondria segmented from cells lacking *TET-YFP-PEX15$_{\Delta C30}$*, with 0 set to the minimum detected autofluorescence density at a mitochondrion. Shown are violin plots of the resulting YFP-Pex15$_{\Delta C30}$ density distributions. Fluorescence densities from 21 cells lacking *YFP-TET-PEX15ΔC30* were measured throughout the timecourse and did not vary dramatically (data not shown), and were thus combined to yield the autofluorescence distribution shown. Dashed line represents 3 standard deviations above the autofluorescence mean. In the *TET-YFP-pex15$_{\Delta C30}$*-containing cells analyzed here, 58 mitochondria out of 2926 (2.0%) displayed fluorescence densities below this 3 standard deviation cutoff. The 515 nm laser

power was increased relative to the experiment in Figure 1 and therefore AUs are not comparable between these experiments.

Figure 3: Pulse-chase analysis of peroxisomal Pex15 turnover by Msp1.

A. Experimental timeline of a pulse-chase analysis similar to the one described in Figure 1A but with 10 μg/ml DOX. This experiment was performed twice with similar results.

B. Representative confocal micrographs from the experiment described in part *A*. Each image represents a maximum intensity projection of a Z-stack. Red cell outlines originate from a single bright-field image acquired at the center of the Z-stack. Scale bar, 5 μm.

C. Quantitation of peroxisomal YFP-Pex15 fluorescence from the experiment described in part *A*. YFP-Pex15 fluorescence density corresponds to the total YFP-Pex15 signal at each computationally-defined peroxisome (marked by mCherry-PTS1) divided by the peroxisomal pixel volume (see Experimental Methods for more details). Shown are violin plots of the resulting YFP-Pex15 density distributions. These data represent analysis of 442 mock-treated and 450 β-estradiol-treated cells followed throughout the time course as well as progeny from cell divisions during the experiment. The 515 nm laser power was decreased relative to the experiments in Figures 1 and 2 and therefore AUs are not comparable between these experiments.

D. Immunoblot analysis of YFP-Pex15 levels after activating *MSP1* expression. Whole cell lysates were prepared from cells grown as described in part *A* at the indicated timepoints after initiating β-estradiol treatment, and then YFP-Pex15 protein was resolved by SDS-PAGE and immunoblotting. Each sample was prepared from an equal volume of culture to

measure turnover of YFP-Pex15 from equivalent amounts of starting material. α-Pgk1 immunoblotting was performed as a loading control.

E. Quantitation of endogenously expressed peroxisomal sfYFP-mCherry-Pex15 (left) or mitochondrial sfYFP-mCherry-Pex15$_{\Delta C30}$ (right) sfYFP fluorescence density in wild-type and *msp1Δ* cells. Peroxisomal sfYFP fluorescence density corresponds to the total sfYFP signal at each computationally-defined peroxisome (marked by mTurquoise2-PTS1). Mitochondrial sfYFP fluorescence density corresponds to the total sfYFP signal at each computationally-defined mitochondrion (marked by Tom70-mTurquoise2). Shown are violin plots of the resulting sfYFP fluorescence density distributions. Background represents the mean auto-fluorescence in the sfYFP channel from peroxisomes and mitochondria in strains lacking fluorescently labeled Pex15. Background is normally distributed around the mean and therefore low-fluorescence or non-fluorescent organelles can have negative fluorescence density after background subtraction. These data represent analysis of 941 sfYFP-mCherry-Pex15 *MSP1* cells, 942 sfYFP-mCherry-Pex15 *msp1Δ* cells, 807 sfYFP-mCherry-Pex15$_{\Delta C30}$ *MSP1* cells, and 918 sfYFP-mCherry-Pex15$_{\Delta C30}$ *msp1Δ* cells.

Figure 3-Figure Supplement 1: Supporting evidence that Msp1 induces turnover of overexpressed Pex15 at peroxisomes.

A. Quantitation of peroxisomal YFP-Pex15 fluorescence density from Figure 3C compared to autofluorescence background. Y axis represents the peroxisomal fluorescence density normalized the mean autofluorescence in peroxisomes from cells lacking *TET-YFP-PEX15*, with 0 set to the minimum detected autofluorescence density at a peroxisome.

Shown are violin plots of the resulting YFP density distributions. Peroxisomes were segmented from 124 cells lacking *TET-YFP-PEX15* throughout the duration of the timecourse to generate the autofluorescence distribution. Dashed line represents 3 standard deviations above the autofluorescence mean. In the *TET-YFP-PEX15*-containing cells analyzed here, 37 peroxisomes out of 4485 (0.8%) displayed fluorescence densities below this 3 standard deviation cutoff. See Figure 3A-C for additional details.

B. Experimental timeline of the staged expression experiment for comparing peroxisomal YFP-Pex15 levels when YFP-Pex15 is produced from the *PEX15* promoter or the *TET* promoter in the presence of varying doxycycline concentrations.

C. Quantitation of peroxisomal YFP-Pex15 fluorescence from the experiment described in part *B*. YFP-Pex15 fluorescence density corresponds to the total YFP-Pex15 signal at each computationally-defined peroxisome (marked by mCherry-PTS1) divided by the peroxisomal pixel volume (see Experimental Methods for more details). Shown are the mean peroxisomal fluorescence densities for each sample normalized to the *PEX15* promoter-driven YFP-Pex15 sample mean. Error bars represent standard error of the population mean.

Figure 4: Experimental and theoretical evidence for the 2-state model of Pex15 turnover at peroxisomes.

A. The apparent difference in the kinetic profiles of Msp1-induced substrate turnover at peroxisomes (Pex15) versus mitochondria ($Pex15_{\Delta C30}$). These data represent quantitation of additional time points from the experiments described in Figure 2 (YFP-$Pex15_{\Delta C30}$) combined with a new experiment to monitor YFP-Pex15 turnover at high temporal

resolution. YFP signal density at mitochondria (red) or peroxisomes (purple) is plotted after normalization to the 0 hour timepoint, with lines directly connecting timepoints. Error bars represent standard error of the mean. These data are reproduced in parts *D* and *F*.

B. Schematics of the two competing models for Pex15 turnover. In the 1-state model, newly-synthesized Pex15 is first targeted and inserted into the peroxisome membrane and then degraded by a simple exponential decay process that occurs with the rate constant k_{decay}. In the 2-state model, there is an additional exponential maturation process that converts Pex15 from a nascent state to a mature state at a rate defined by k_{mat}. In addition, this model includes the new exponential decay constant $k_{decay,2}$ for the mature Pex15 state that is distinct from the $k_{decay,1}$ of the nascent state.

C. Experimental timeline of the staged expression experiment for monitoring Msp1-dependent turnover of mitochondrial $Pex15_{\Delta C30}$ with high temporal resolution. 50 µg/ml DOX was used for induction.

D. Quantitation of mitochondrial YFP-$Pex15_{\Delta C30}$ fluorescence from the experiment described in part *C*. YFP signal density at mitochondria was determined as described in Figure 1 and plotted after normalization to the 0 hour timepoint. Error bars represent standard error of the mean. Data were fitted to the competing models described in part *B* as indicated (See Experimental Methods for model fitting details). See Figure 4-Figure Supplement 1C for fit parameters.

E. Schematic of the staged expression experiment for monitoring Msp1-dependent turnover of peroxisomal Pex15 with high temporal resolution. 10 µg/ml DOX was used for induction. This experiment was performed three times with similar results.

F. Quantitation of peroxisomal YFP-Pex15 fluorescence from the experiment described in part *E*. YFP signal density at peroxisomes was determined as described in Figure 3C and plotted as in part *D*. The inset shows model fitting with later timepoints included. See Figure 4-Figure Supplement 1C for fit parameters. See Figure 4-Figure Supplement 1B for two additional experimental replicates.

Figure 4-Figure Supplement 1: Supporting evidence for the 2-state model of Pex15 turnover at peroxisomes.

A. Quantitation of the fraction of mitochondria lacking detectable YFP fluorescence from the experiment described in Figure 4A,C-D. The Y axis represents the fraction of *TET-YFP-pex15ΔC30* mitochondria with fluorescence values less than two standard deviations above the mean autofluorescence background. Model fitting was disrupted if >5% of organelles (dashed red line) did not contain detectable signal, and therefore model fitting was only performed through the one hour timepoint for YFP-Pex15$_{\Delta C30}$ turnover. All *TET-YFP-PEX15* peroxisomes analyzed in Figure 4A,E-F contained detectable YFP fluorescence (data not shown).

B. Quantitation of peroxisomal fluorescence densities in additional experimental replicates for the experiment described in Figure 4A,E-F. Replicate 1 represents the same data shown in Figure 4A,E-F. Error bars represent standard error of the population mean. See Figure 4E-F for additional details.

C. Fit quality and parameters from model fits shown in Figures 4D and 4F. RSS, residual sum of squares. Probability that the 2-state model provided the better fit was calculated by comparing the Akaike Information Criteria between the 1-state and 2-state fits (see

Experimental Methods for additional details). Reported rate constants represent the values provided by the better fit, with 95% confidence intervals displayed in parentheses. n.a. indicates where rate constants are not appropriate. Red color highlights the strong statistical preference for the 2-state model as a fit of turnover data for peroxisomal Pex15 following β-estradiol-induced Msp1 expression.

Figure 5: Experimental measurement of Pex15 levels and age after Msp1 activation compared to theoretical modeling.

A. Schematic of the staged expression experiment for monitoring turnover of sfYFP-mCherry-Pex15 expressed from the native genomic *PEX15* promoter following Msp1 overexpression.

B. Simulations of for mCherry/sfYFP ratio (top) and Pex15 decay (bottom) as a function of time following Msp1 activation in a 1-state or 2-state regime. Different colors show Pex15 dynamics resulting from the indicated theoretical half-life parameters. See Experimental Methods for simulation details.

C. Experimentally measured mCherry/sfYFP ratio (top) and sfYFP density decay (bottom) from the experiment described in part *B*. Error bars represent standard error of the mean. Greater than 100 cells were imaged for each sample at each time point, and different fields of cells were imaged at each time point to minimize photobleaching. This experiment was performed twice with similar results.

Figure 5-Figure Supplement 1: Supporting information for tandem fluorescent timer-tagged Pex15.

A. Tandem fluorescent timer schematics. Pex15 is N-terminally tagged with a superfolding YFP (sfYFP) followed by mCherry. sfYFP matures with a half-time of ~10 minutes (Hansen and O'Shea, 2013), whereas mCherry matures with a half-time of ~40 minutes (Khmelinskii et al., 2012).

B. Theoretical fraction of sfYFP molecules and mCherry molecules that are fluorescent at indicated times following synthesis as well as the ratio of mCherry:sfYFP fluorescence signal. Curves calculated based on maturation rates in *A*.

Figure 6: Pex3 protects Pex15 from Msp1-induced turnover.

A. Wild-type and *msp1Δ* cells containing the doxycycline-inducible promoter driving YFP-Pex15 expression (*pTET-YFP-PEX15)* and expressing Pex3-AID were grown for 3 hours in the presence of 10 µg/ml doxycycline (DOX) before they were washed and grown for 2 hours in drug-free media. Following this period of substrate pre-loading, half of the cells were exposed to 1 mM Auxin, followed by time-lapse imaging of both cell populations using a spinning disk confocal microscope. This experiment was performed three times with similar results.

B. Quantitation of peroxisomal YFP-Pex15 fluorescence from the experiment described in part *A*. YFP signal density at peroxisomes was determined as described in Figure 2 and plotted after normalization to the –Auxin sample value at the 0 hour timepoint of the corresponding strain. Error bars represent standard error of the mean. These data represent analysis of 299 mock-treated *MSP1* cells, 344 Auxin-treated *MSP1* cells, 314 mock-treated *msp1Δ* cells, and 203 Auxin-treated *msp1Δ* cells followed throughout the time course as well as progeny from cell divisions during the experiment.

Figure 6-Figure Supplement 1: Supporting evidence for Pex15 interaction with Pex3 and rapid *in situ* destruction of Pex3-AID.

A. Quantitation of peroxisomal sfYFP-mCherry-Pex15 sfYFP fluorescence density in wild-type, *pex1Δ*, and *pex6Δ* cells. sfYFP fluorescence density corresponds to the total sfYFP-mCherry-Pex15 (produced from its native promoter and integrated at the *URA3* locus) signal at each computationally-defined peroxisome (marked by Pex11-mTurquoise2) divided by the organelle's pixel volume (see Experimental Methods for more details). Shown are the mean fluorescence densities for each sample normalized to the wild-type mean. Error bars represent standard error of the population mean.

B. Whole cell lysates prepared from *PEX3 msp1Δ* and *PEX3-FLAG msp1Δ* cells expressing tFT-Pex15 from its native genomic promoter were solubilized with NP-40 and then incubated with anti-FLAG resin. The resulting immunoprecipitates (IP) were washed and then eluted with FLAG peptide. Elutions and IP inputs (10%) were resolved by SDS-PAGE and analyzed by immunoblotting with the indicated antibodies (see Experimental Methods for details).

C. Quantitation of peroxisomal YFP-Pex15 fluorescence density at timepoint 0 in wild-type and *msp1Δ* -Auxin samples from Figure 4B. Peroxisomal fluorescence density corresponds to the total YFP fluorescence signal at each computationally-defined peroxisome (marked by mCherry-PTS1) divided by the pixel volume of the peroxisome. Error bars represent standard error of the mean. See Figure 6 for additional details.

D. Confocal micrographs of cells producing C-terminally GFP-AID tagged Pex3 from its native locus in the presence and absence of 1 mM Auxin treatment for 1 hour. mCherry-

PTS1 was produced constitutively from a strong promoter at the *TRP1* locus and OsTir1 was produced constitutively from a strong promoter at the *LEU2* locus (see Experimental Methods for strain details). Each image represents a maximum intensity projection of a Z-stack. Red cell outlines originate from a single bright-field image acquired at the center of the Z-stack. Below, quantitation of the fraction of peroxisomes containing GFP fluorescence in the presence and absence of Auxin treatment. Scale bar, 5 μm. n.d., none detected.

E. Cells expressing Pex3-V5-AID (from the native locus) and OsTIR1 (from a transgene at the *LEU2* locus) as indicated were treated with Auxin for the indicated times prior to whole-cell lysate preparation. Samples were resolved by SDS-PAGE and analyzed by immunoblotting with the indicated antibodies. Hsc82 is an abundant chaperone that served as a loading control.

F. Western blotting analysis similar to the one described in part E but with the additional use of cycloheximide (CHX) as indicated. Pgk1 is an abundant glycolytic enzyme that served as a loading control.

G. Western blotting analysis similar to the one described in part E comparing Pex3-V5-AID turnover in the presence and absence of Msp1. Pgk1 is an abundant glycolytic enzyme that served as a loading control.

Figure 7: Model for substrate selection by Msp1.

On the left, mistargeted Pex15 inserts into mitochondria and is then recognized by Msp1 for extraction. On the right, following insertion into peroxisomes, nascent Pex15 can be recognized by Msp1 in principle but in practice this requires either Pex15 and/or Msp1 to

be present above their usual levels. Otherwise, normal Msp1 recognition is slow relative to the faster "maturation" process involving Pex3 interaction with Pex15, which blocks Msp1 recognition.

Figure 1

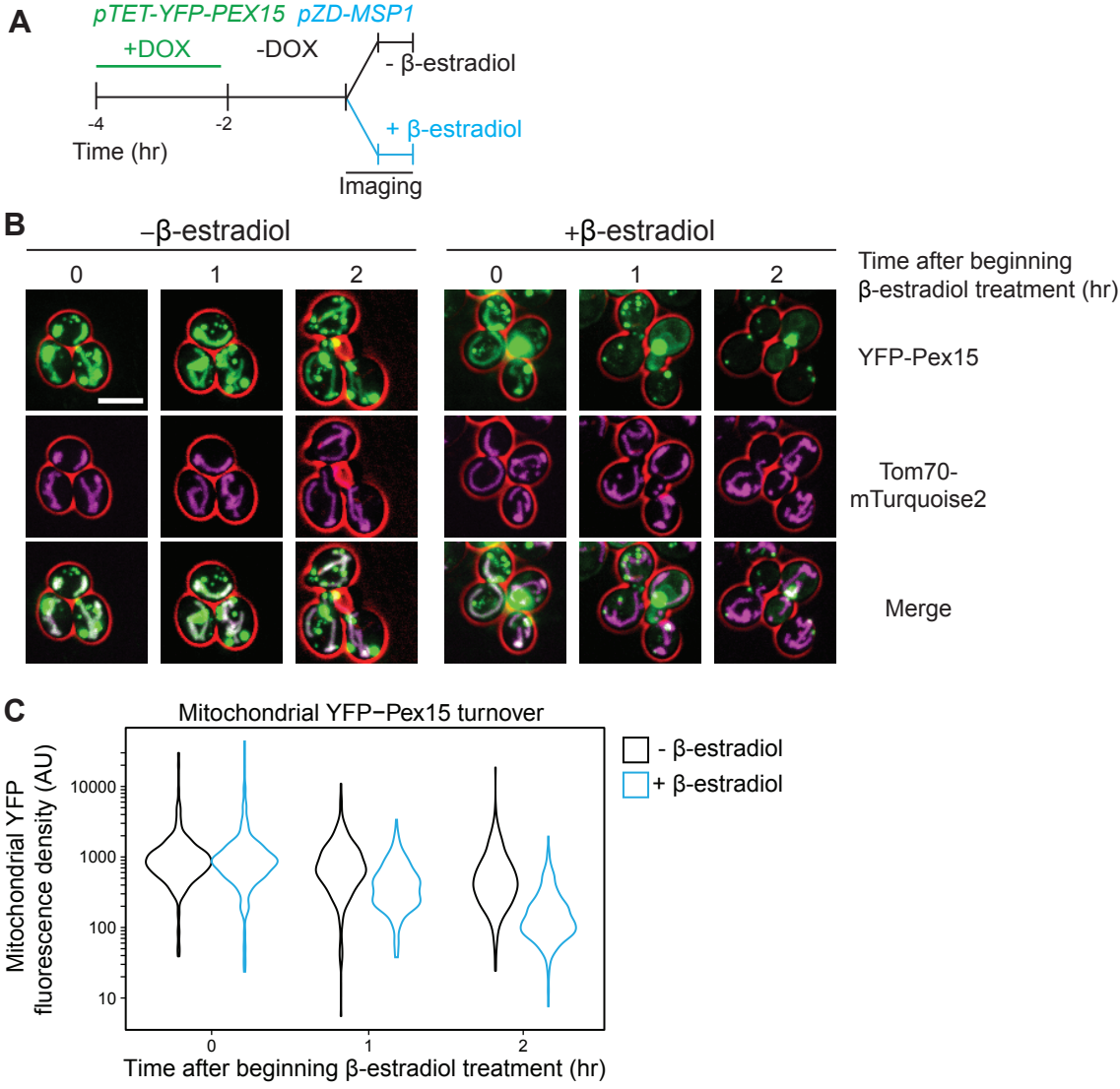
A
pTET-YFP-PEX15
pZD-MSP1
+DOX
-DOX
- β-estradiol
+ β-estradiol
-4
-2
Time (hr)
Imaging
B
−β-estradiol
+β-estradiol
0
1
2
0
1
2
Time after beginning β-estradiol treatment (hr)
YFP-Pex15
Tom70-mTurquoise2
Merge
C
Mitochondrial YFP−Pex15 turnover
Mitochondrial YFP fluorescence density (AU)
10000
1000
100
10
- β-estradiol
+ β-estradiol
0
1
2
Time after beginning β-estradiol treatment (hr)

Figure 1-Figure Supplement 1

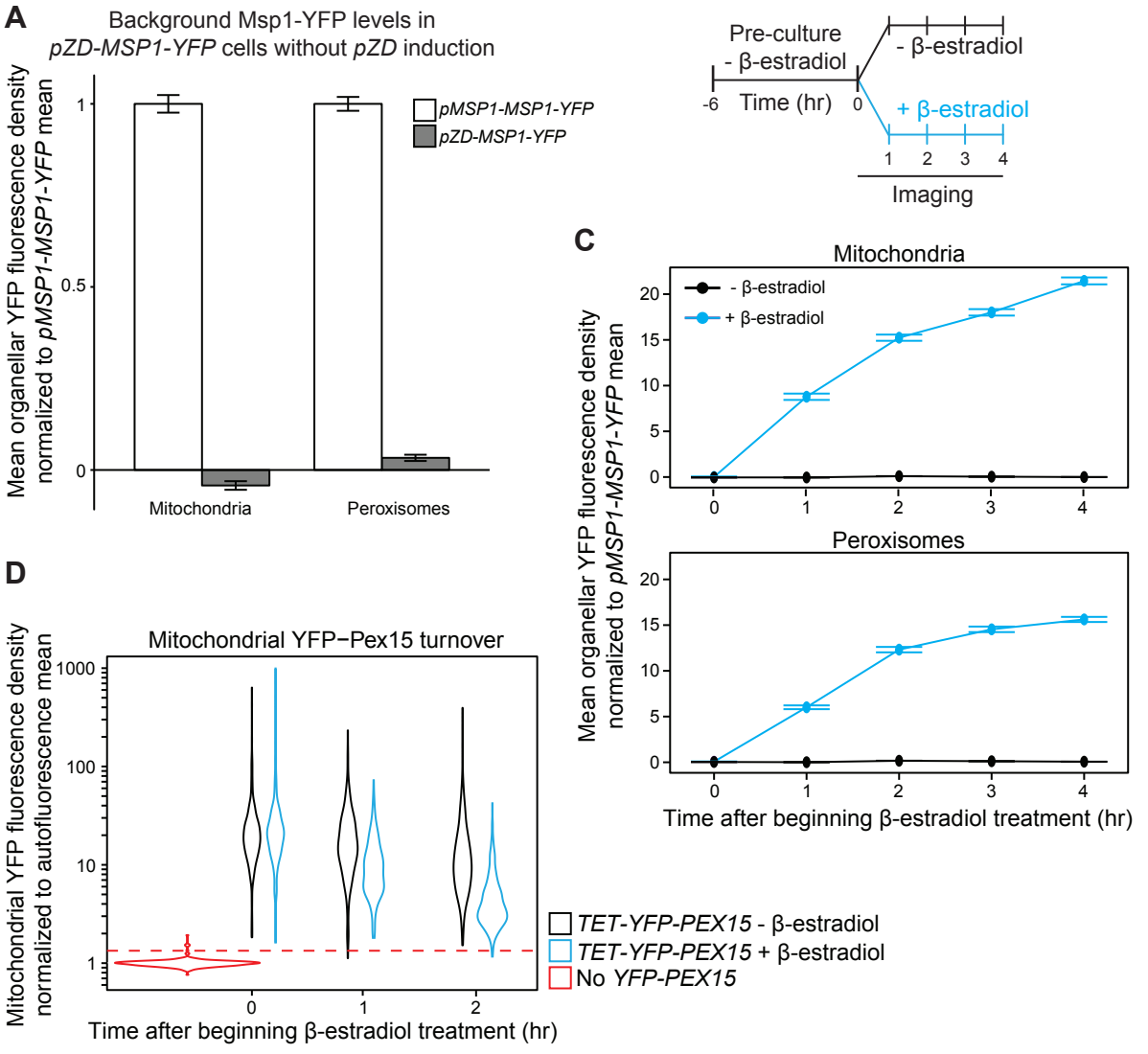

Figure 1-Figure Supplement 2

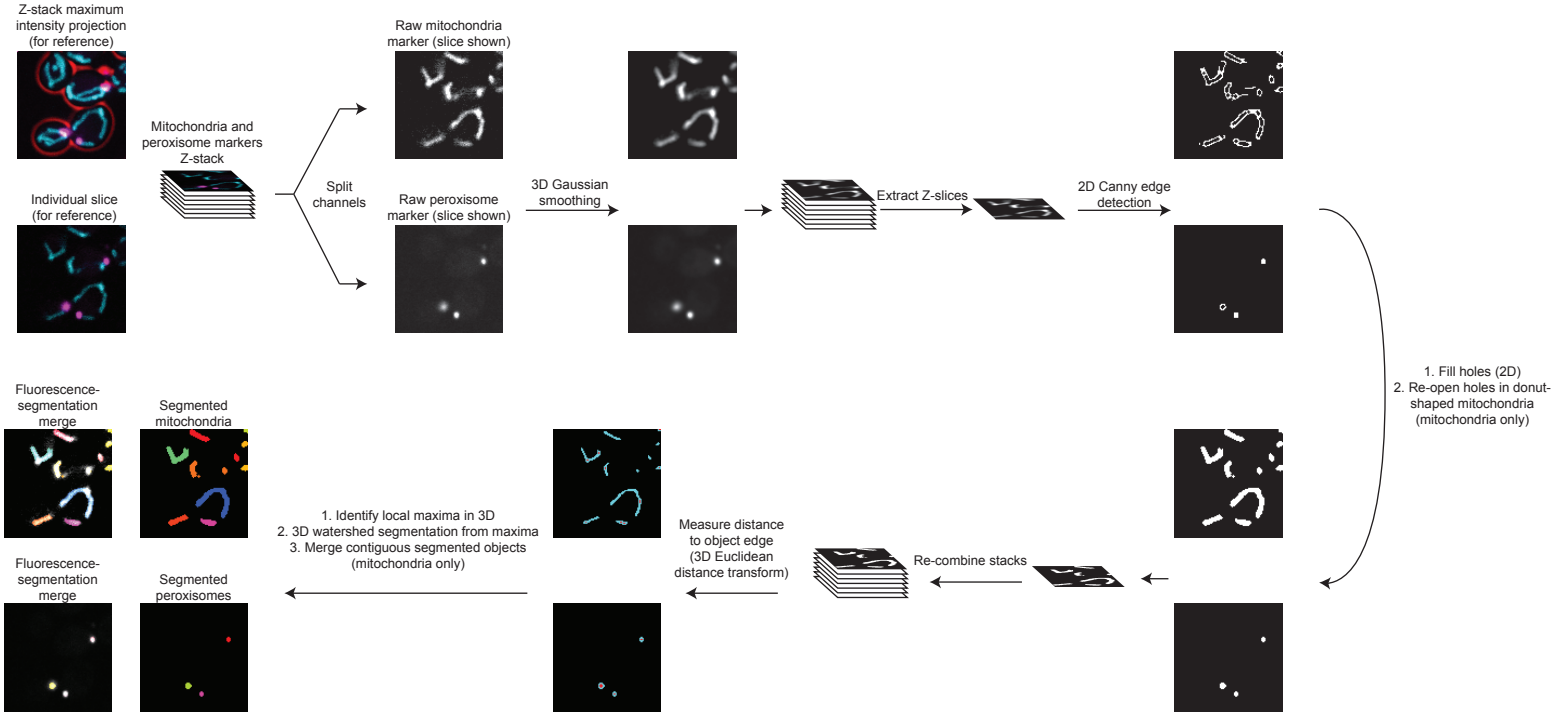

Figure 2

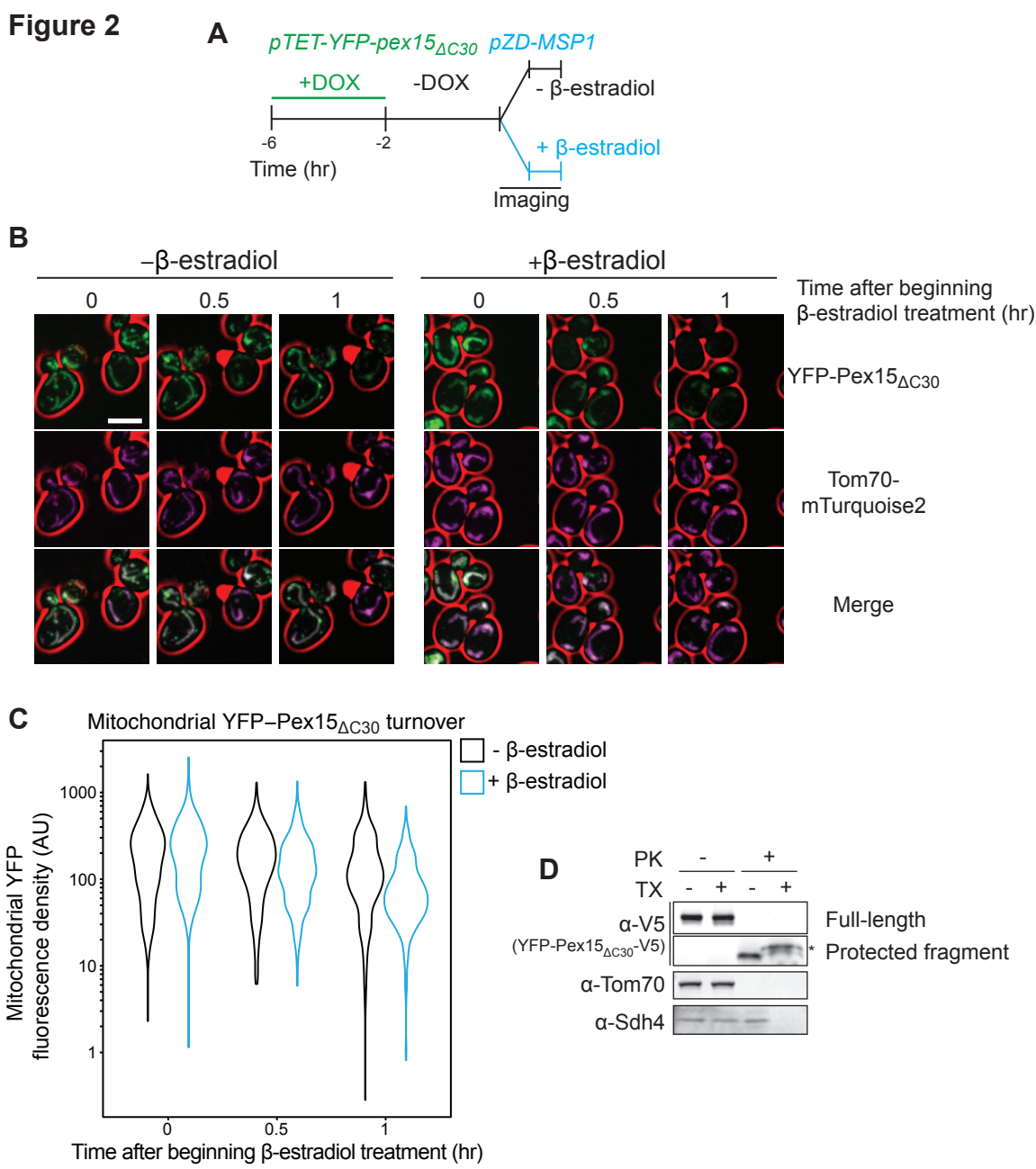
A
pTET-YFP-pex15ΔC30
pZD-MSP1
+DOX
-DOX
- β-estradiol
+ β-estradiol
-6
-2
Time (hr)
Imaging
B
–β-estradiol
+β-estradiol
0
0.5
1
0
0.5
1
Time after beginning β-estradiol treatment (hr)
YFP-Pex15ΔC30
Tom70-mTurquoise2
Merge
C
Mitochondrial YFP–Pex15ΔC30 turnover
- β-estradiol
+ β-estradiol
Mitochondrial YFP fluorescence density (AU)
1000
100
10
1
0
0.5
1
Time after beginning β-estradiol treatment (hr)
D
PK
TX
α-V5
(YFP-Pex15ΔC30-V5)
α-Tom70
α-Sdh4
Full-length
Protected fragment

Figure 2-Figure Supplement 1

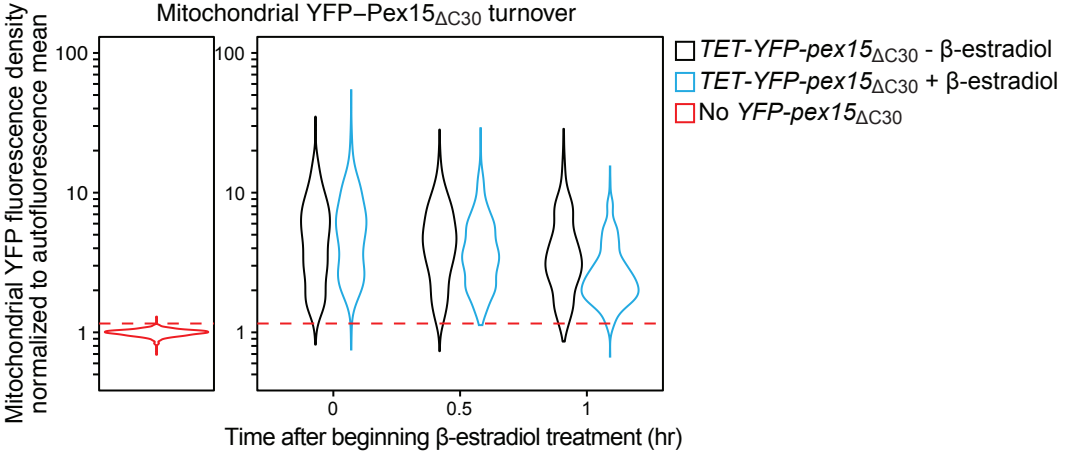

Figure 3

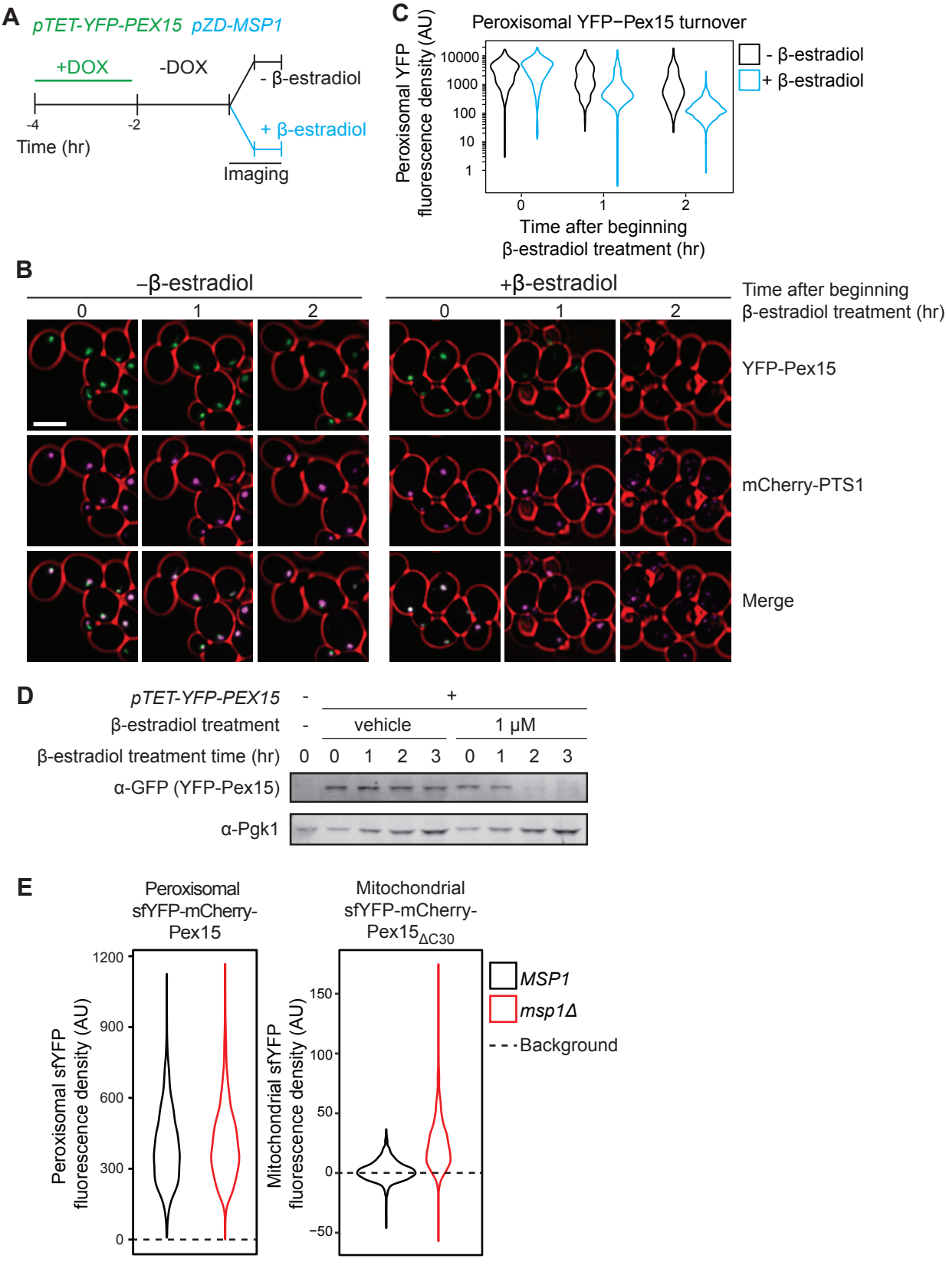
A
pTET-YFP-PEX15 pZD-MSP1
+DOX
-DOX
- β-estradiol
+ β-estradiol
-4
-2
Time (hr)
Imaging
C
Peroxisomal YFP−Pex15 turnover
Peroxisomal YFP fluorescence density (AU)
10000
1000
100
10
1
0
1
2
Time after beginning β-estradiol treatment (hr)
- β-estradiol
+ β-estradiol
B
−β-estradiol
+β-estradiol
0
1
2
Time after beginning β-estradiol treatment (hr)
YFP-Pex15
mCherry-PTS1
Merge
D
pTET-YFP-PEX15
β-estradiol treatment
vehicle
1 μM
β-estradiol treatment time (hr)
0 0 1 2 3 0 1 2 3
α-GFP (YFP-Pex15)
α-Pgk1
E
Peroxisomal sfYFP-mCherry-Pex15
Mitochondrial sfYFP-mCherry-Pex15ΔC30
Peroxisomal sfYFP fluorescence density (AU)
1200
900
600
300
0
Mitochondrial sfYFP fluorescence density (AU)
150
100
50
0
−50
MSP1
msp1Δ
Background

Figure 3-Figure Supplement 1

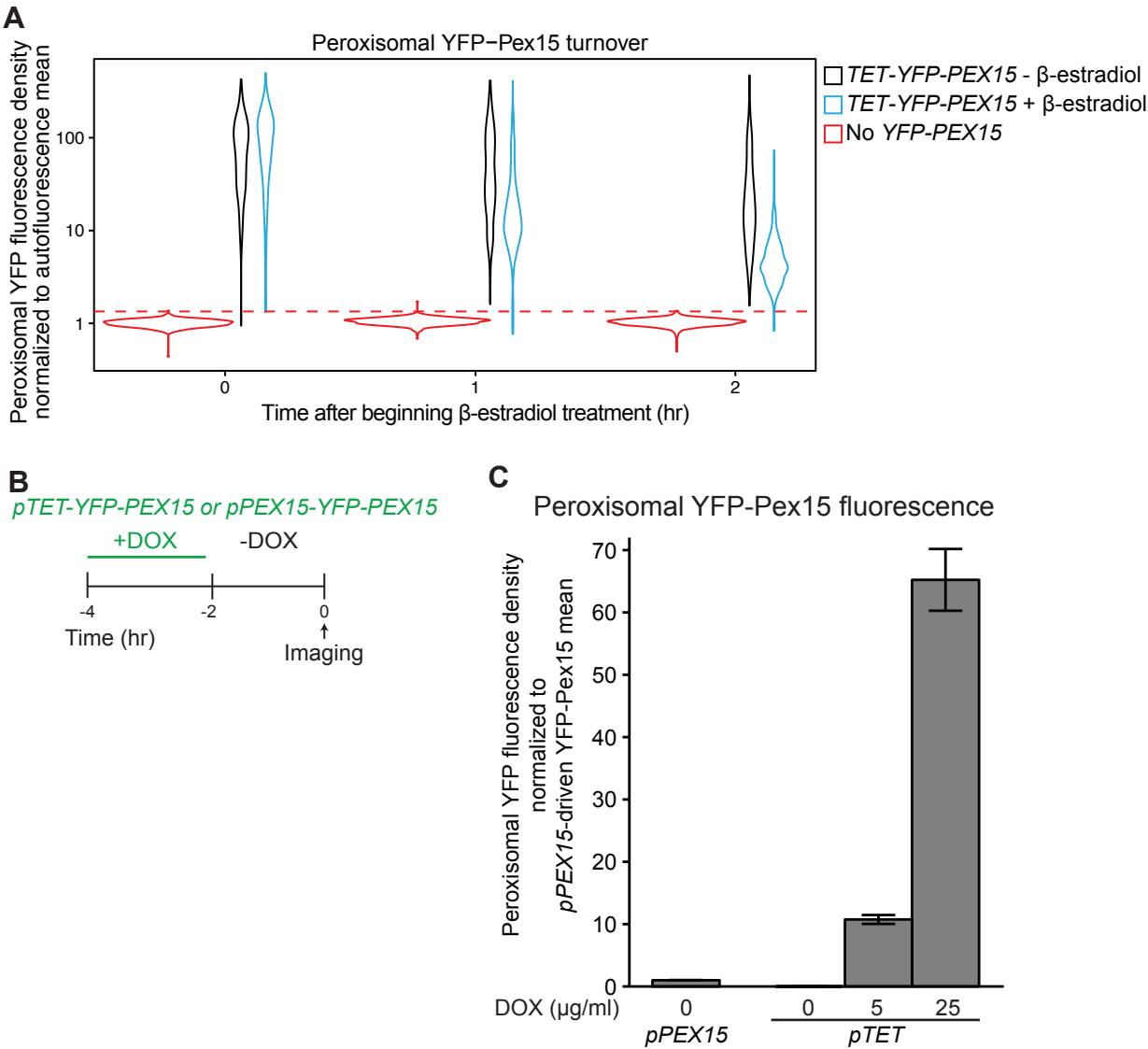

Figure 4

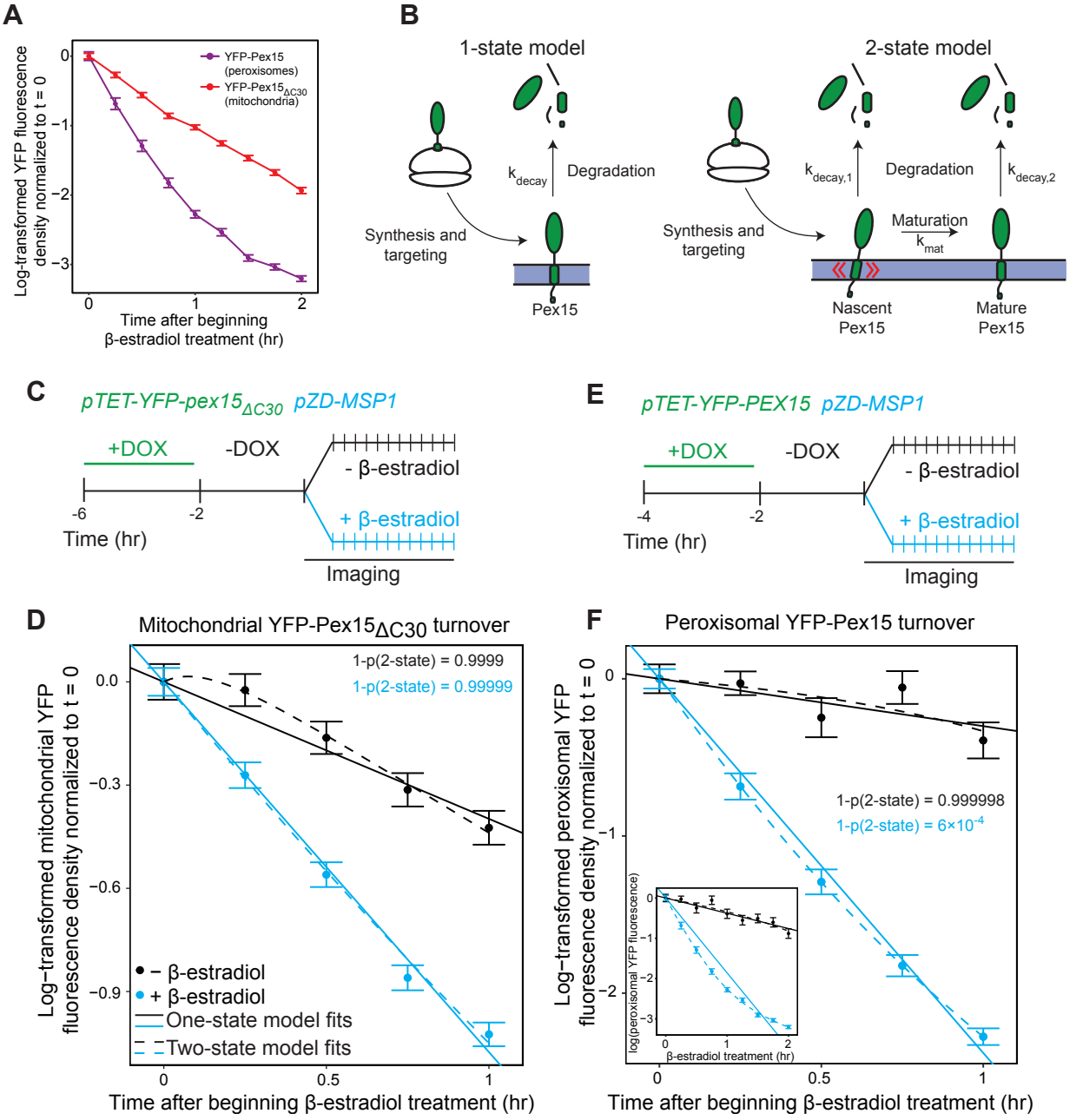
A
Log-transformed YFP fluorescence density normalized to t = 0
YFP-Pex15 (peroxisomes)
YFP-Pex15ΔC30 (mitochondria)
Time after beginning β-estradiol treatment (hr)
B
1-state model
k_decay
Degradation
Synthesis and targeting
Pex15
2-state model
k_decay,1
Degradation
k_decay,2
Synthesis and targeting
Maturation
k_mat
Nascent Pex15
Mature Pex15
C
pTET-YFP-pex15ΔC30 pZD-MSP1
+DOX
-DOX
- β-estradiol
+ β-estradiol
Time (hr)
Imaging
E
pTET-YFP-PEX15 pZD-MSP1
+DOX
-DOX
- β-estradiol
+ β-estradiol
Time (hr)
Imaging
D
Mitochondrial YFP-Pex15ΔC30 turnover
1-p(2-state) = 0.9999
1-p(2-state) = 0.99999
Log−transformed mitochondrial YFP fluorescence density normalized to t = 0
− β-estradiol
+ β-estradiol
One-state model fits
Two-state model fits
Time after beginning β-estradiol treatment (hr)
F
Peroxisomal YFP-Pex15 turnover
1-p(2-state) = 0.999998
1-p(2-state) = 6×10^-4
Log−transformed peroxisomal YFP fluorescence density normalized to t = 0
log(peroxisomal YFP fluorescence)
β-estradiol treatment (hr)
Time after beginning β-estradiol treatment (hr)

Figure 4-Figure Supplement 1

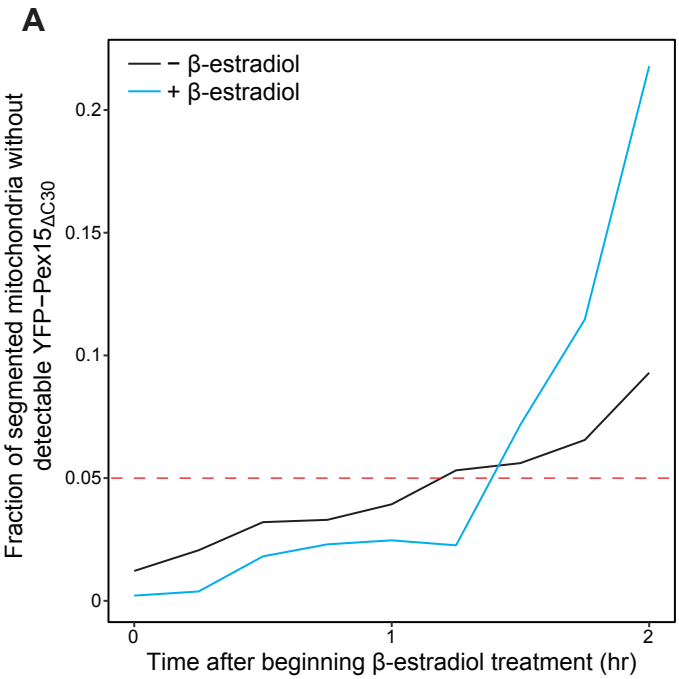

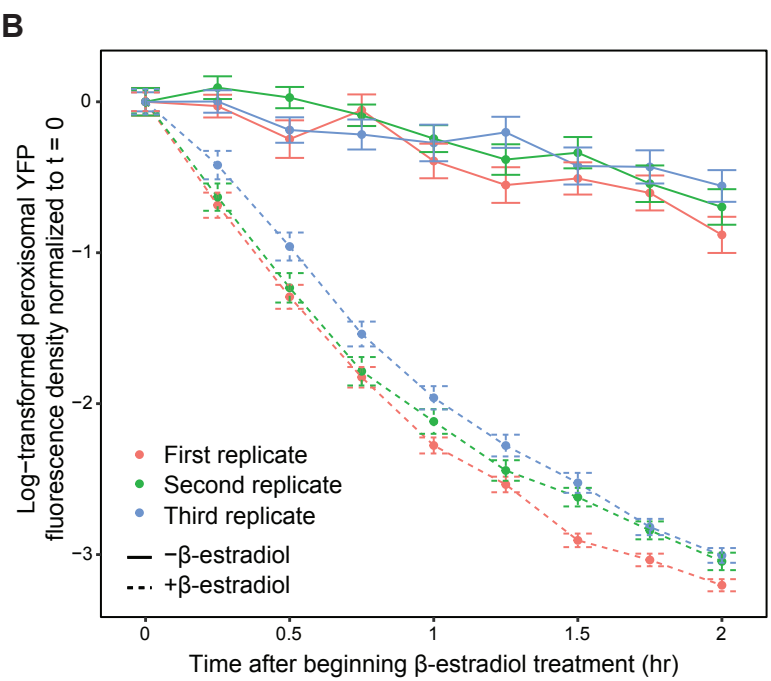

C

	Mitochondrial YFP-Pex15$_{\Delta C30}$		Peroxisomal YFP-Pex15	
	- β-estradiol	**+ β-estradiol**	**- β-estradiol**	**+ β-estradiol**
$RSS_{1\text{-state}}$	0.00797	0.00596	0.0488	0.0308
$RSS_{2\text{-state}}$	0.00142	0.00377	0.0441	7.78×10^{-6}
1-p(2-state)	0.9999	0.99999	0.999998	6×10^{-4}
Pref. model	**1-state**	**1-state**	**1-state**	**2-state**
k_{decay}	0.398 (0.308, 0.489)	1.076 (0.998, 1.154)	0.301 (0.077, 0.525)	n.a.
$k_{decay,1}$	n.a.	n.a.	n.a.	2.86 (2.80, 2.93)
$k_{decay,2}$	n.a.	n.a.	n.a.	1.09 (0.70, 1.40)
k_{mat}	n.a.	n.a.	n.a.	0.524 (0.314, 0.834)

Figure 5

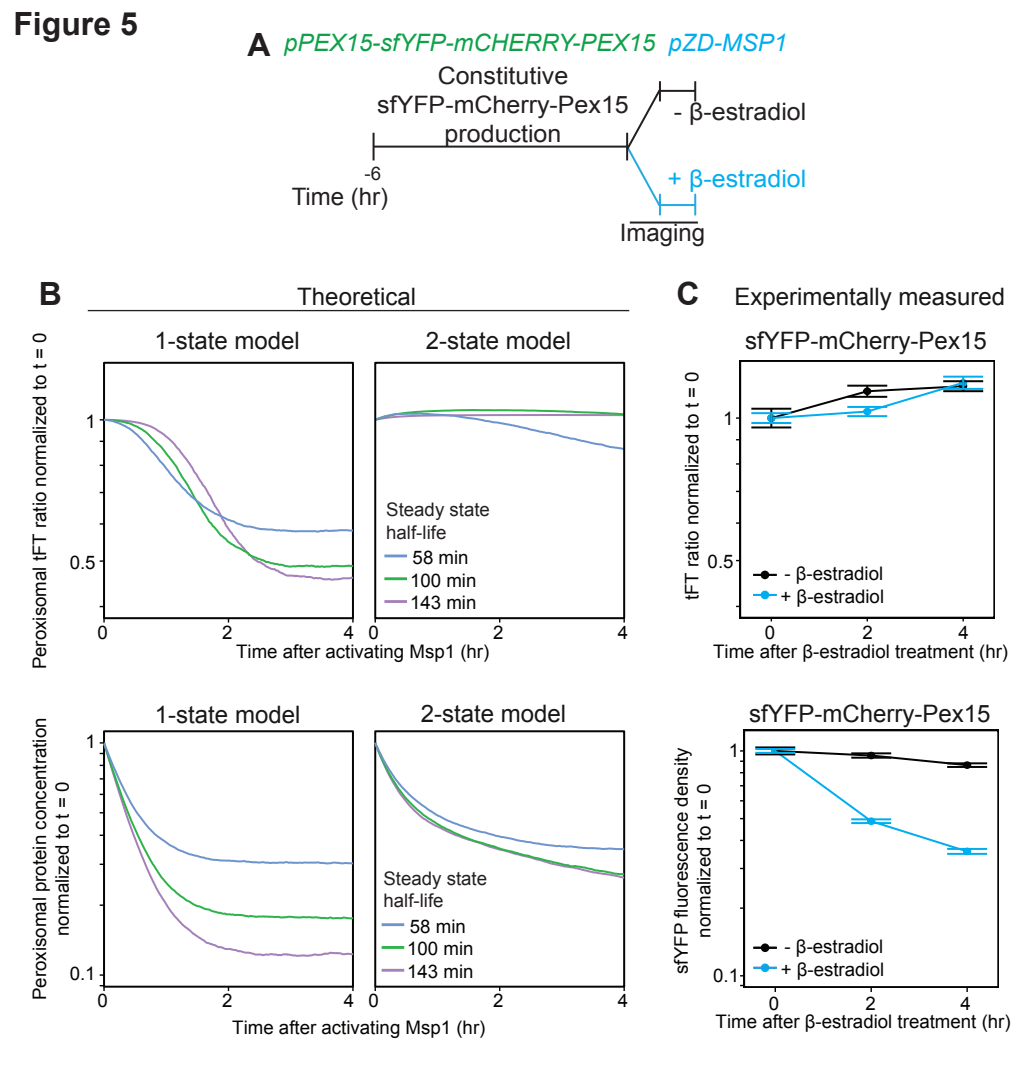
A
pPEX15-sfYFP-mCHERRY-PEX15
pZD-MSP1
Constitutive
sfYFP-mCherry-Pex15
production
- β-estradiol
+ β-estradiol
-6
Time (hr)
Imaging
B
Theoretical
1-state model
2-state model
Peroxisomal tFT ratio normalized to t = 0
Steady state
half-life
58 min
100 min
143 min
Time after activating Msp1 (hr)
Peroxisomal protein concentration
normalized to t = 0
C
Experimentally measured
sfYFP-mCherry-Pex15
tFT ratio normalized to t = 0
- β-estradiol
+ β-estradiol
Time after β-estradiol treatment (hr)
sfYFP fluorescence density
normalized to t = 0

Figure 5-Figure Supplement 1

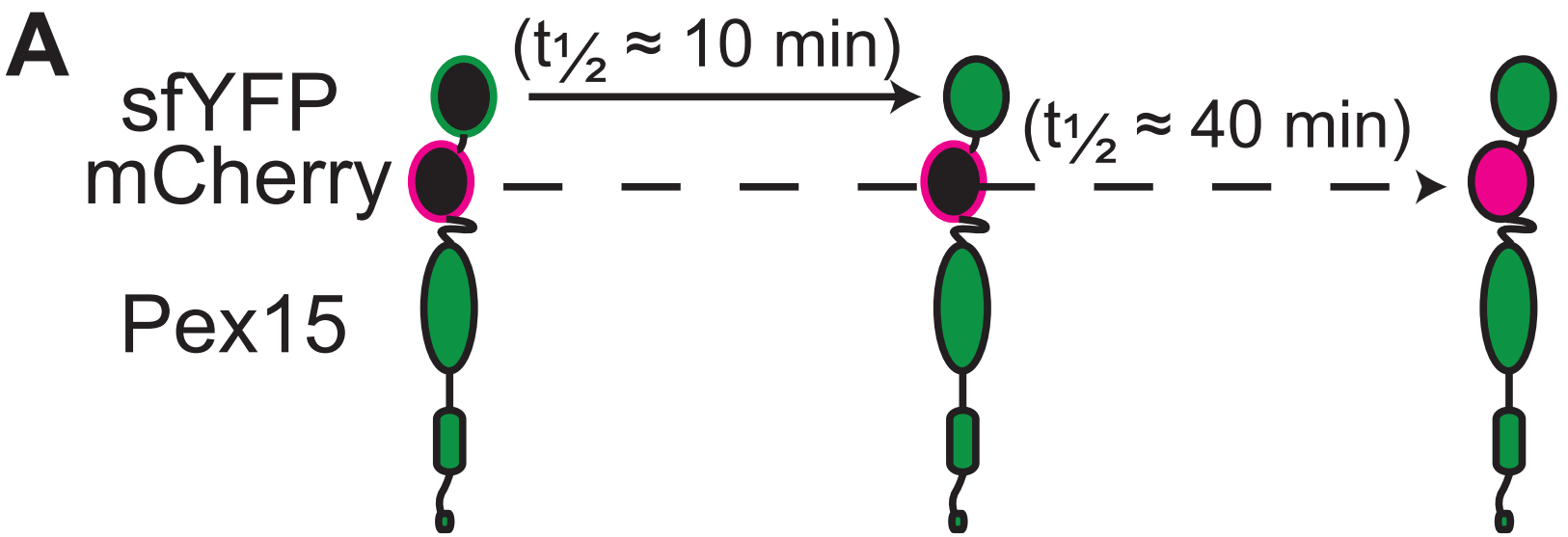

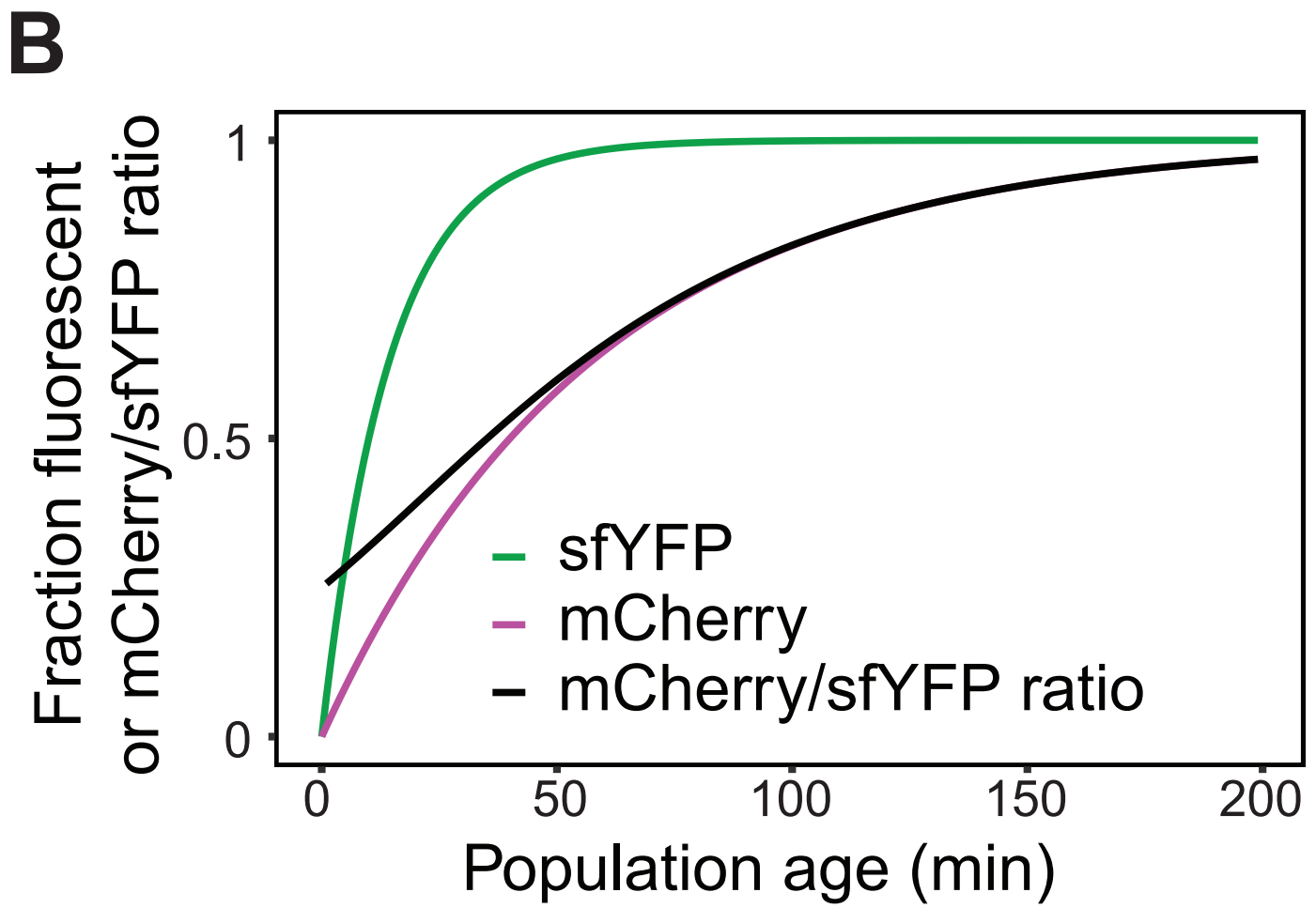

Figure 6

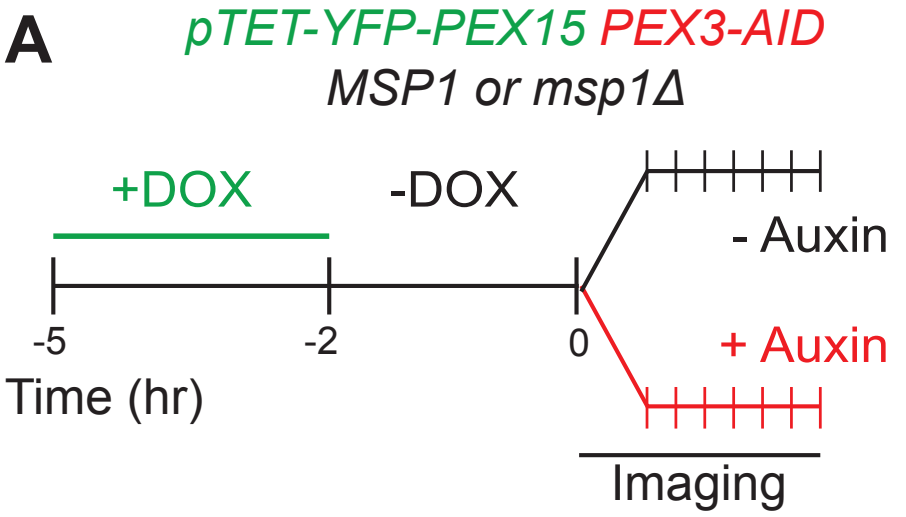
A
pTET-YFP-PEX15 PEX3-AID
MSP1 or msp1Δ
+DOX
-DOX
- Auxin
+ Auxin
-5
-2
0
Time (hr)
Imaging

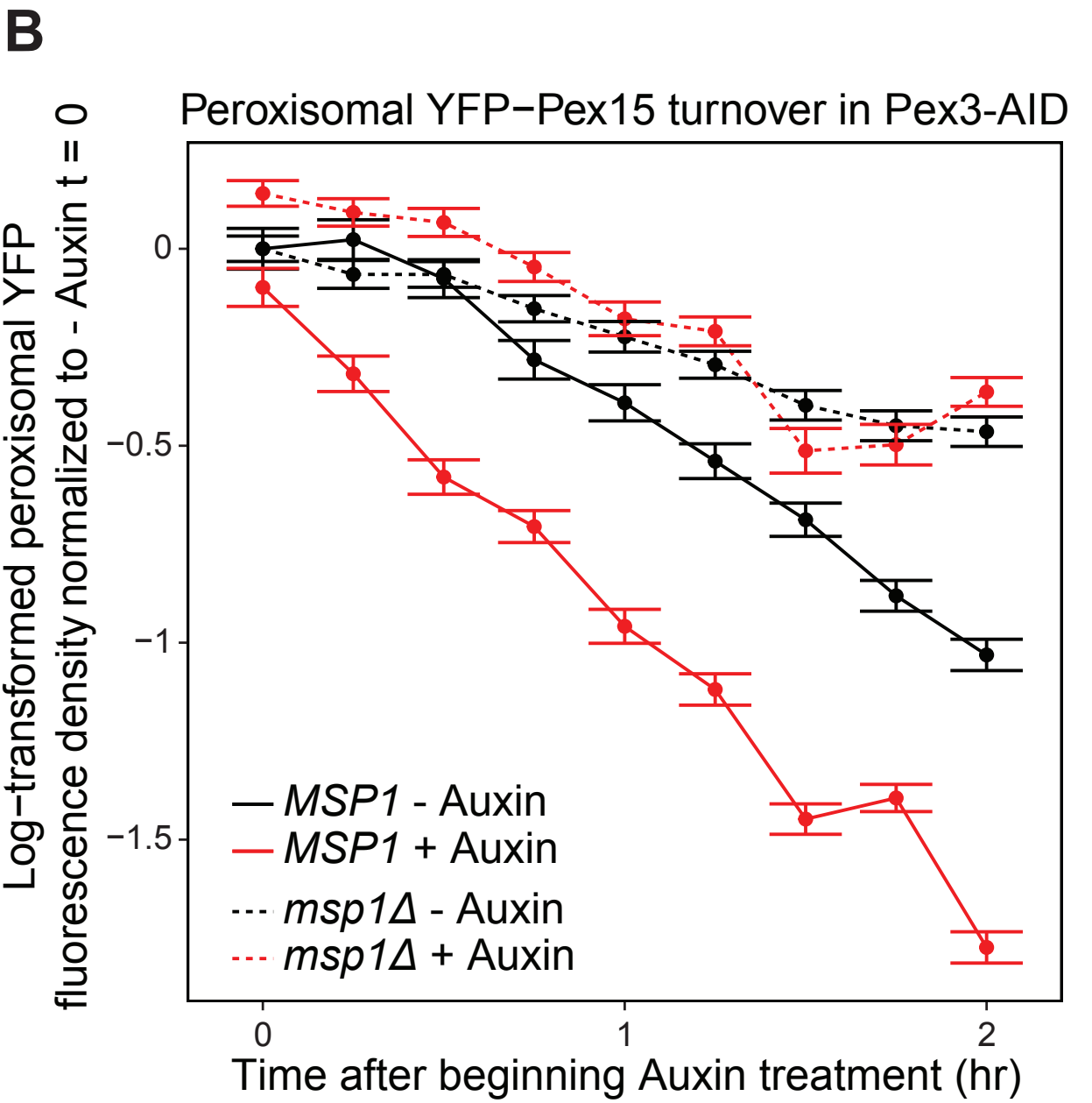
B
Peroxisomal YFP−Pex15 turnover in Pex3-AID
Log−transformed peroxisomal YFP fluorescence density normalized to - Auxin t = 0
0
−0.5
−1
−1.5
MSP1 - Auxin
MSP1 + Auxin
msp1Δ - Auxin
msp1Δ + Auxin
0
1
2
Time after beginning Auxin treatment (hr)

Figure 6-Figure Supplement 1

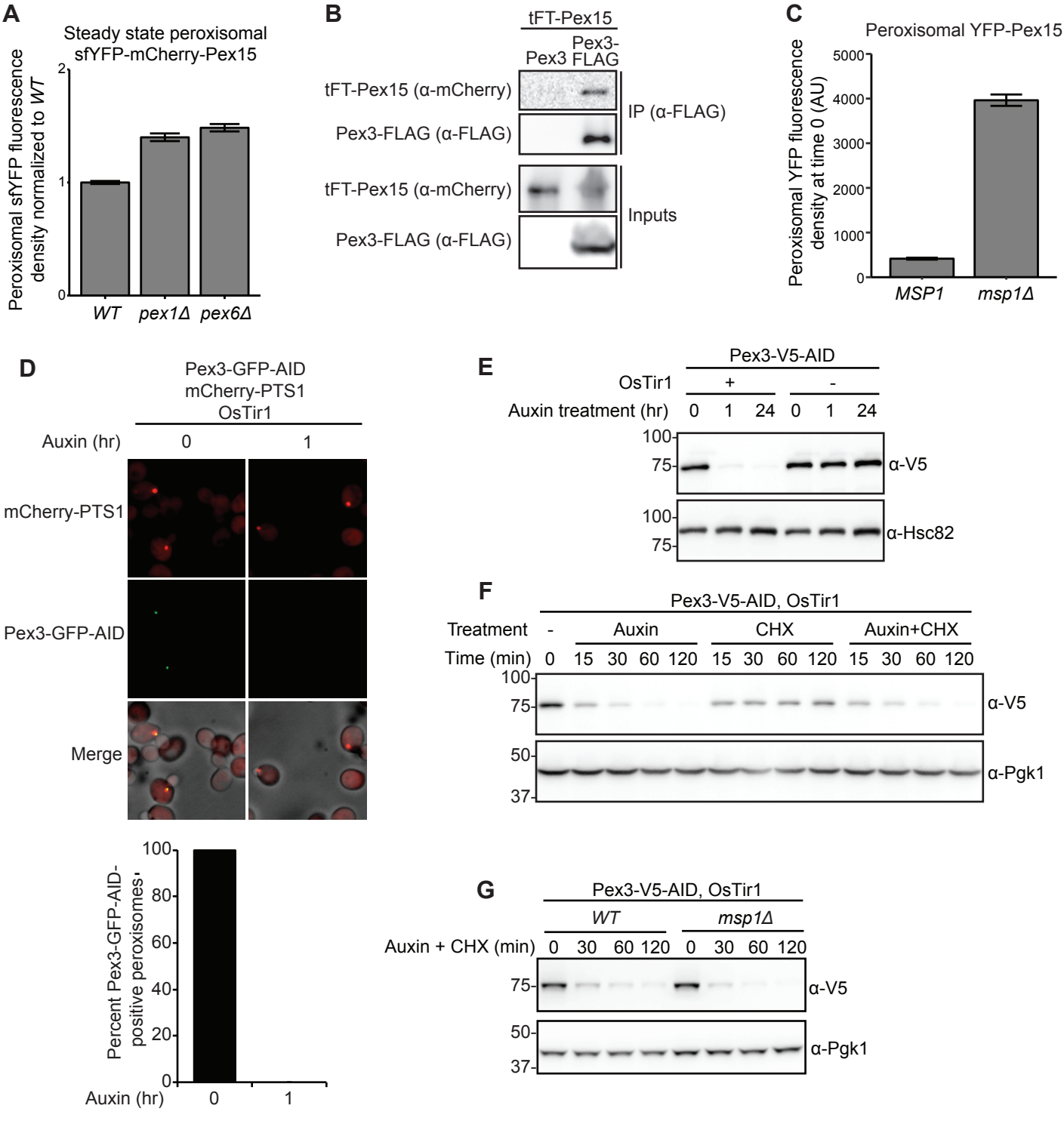

Figure 7

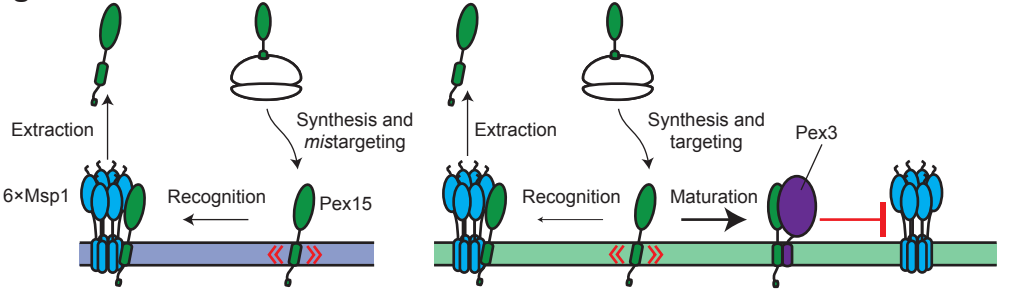
Extraction
Synthesis and
*mis*targeting
6×Msp1
Recognition
Pex15
Mitochondrial outer membrane
Extraction
Synthesis and
targeting
Pex3
Recognition
Maturation
Peroxisomal membrane

Strain Table

S. cerevisiae: Strain *BY4741*	(Baker Brachmann et al., 1998)	Euroscarf
S. cerevisiae: Strain *BY4741 trp1Δ::pTDH3-mTURQUOISE2-PTS1-SpHIS5*	This study	VDY3349
S. cerevisiae: Strain *trp1Δ::pTDH3-mTURQUOISE2-PTS1-SpHIS5 ura3Δ::pPEX15-sfYFP-mCHERRY-PEX15-tPEX15-KANMX*	This study	VDY3350
S. cerevisiae: Strain *trp1Δ::pTDH3-mTURQUOISE2-PTS1-SpHIS5 ura3Δ::pPEX15-sfYFP-mCHERRY-PEX15-tPEX15-KANMX msp1Δ::HPHMX*	This study	VDY3351
S. cerevisiae: Strain *trp1Δ::pTDH3-mTURQUOISE2-PTS1-SpHIS5 ura3Δ::pPEX15-sfYFP-mCHERRY-PEX15-tPEX15-KANMX CgLEU2-Z4EV-pZD-MSP1*	This study	VDY3352
S. cerevisiae: Strain *trp1Δ::pTDH3-mTURQUOISE2-PTS1-SpHIS5 ura3Δ::pPEX15-sfYFP-mCHERRY-PEX15-tPEX15-KANMX msp1Δ::HPHMX PEX3-3FLAG-NATMX*	This study	VDY3353
S. cerevisiae: Strain *BY4741 TOM70-mTURQUOISE2-SpHIS5*	This study	VDY3354
S. cerevisiae: Strain *BY4741 TOM70-mTURQUOISE2-SpHIS5 ura3Δ::pPEX15-sfYFP-mCHERRY-pex15$_{\Delta C30}$-tPEX15-KANMX*	This study	VDY3355
S. cerevisiae: Strain *BY4741 TOM70-mTURQUOISE2-SpHIS5 ura3Δ::pPEX15-sfYFP-mCHERRY-pex15$_{\Delta C30}$-tPEX15-KANMX msp1Δ::HPHMX*	This study	VDY3356
S. cerevisiae: Strain *BY4741 TOM70-mTURQUOISE2-SpHIS5 trp1Δ::pTDH3-mCHERRY-PTS1-CgURA3*	This study	VDY3357
S. cerevisiae: Strain *BY4741 TOM70-mTURQUOISE2-SpHIS5 trp1Δ::pTDH3-mCHERRY-PTS1-CgURA3 MSP1-YFP-KANMX*	This study	VDY3358
S. cerevisiae: Strain *BY4741 TOM70-mTURQUOISE2-SpHIS5 trp1Δ::pTDH3-mCHERRY-PTS1-CgURA3 CgLEU2-Z4EV-pZD-MSP1-YFP-KANMX*	This study	VDY3359
S. cerevisiae: Strain *BY4741 TOM70-mTURQUOISE2-SpHIS5 trp1Δ::pTDH3-mCHERRY-PTS1-CgURA3 CgLEU2-Z4EV-pZD-MSP1*	This study	VDY3360
S. cerevisiae: Strain *BY4741 TOM70-mTURQUOISE2-SpHIS5 trp1Δ::pTDH3-mCHERRY-PTS1-CgURA3 CgLEU2-Z4EV-pZD-MSP1 ura3Δ::CgTRP1-rTA-pTET-YFP-PEX15-tPEX15*	This study	VDY3361
S. cerevisiae: Strain *BY4741 TOM70-mTURQUOISE2-SpHIS5 trp1Δ::pTDH3-mCHERRY-PTS1-CgURA3 CgLEU2-Z4EV-pZD-MSP1 ura3Δ::CgTRP1-rTA-pTET-YFP-pex15$_{\Delta C30}$-tPEX15*	This study	VDY3362
S. cerevisiae: Strain *BY4741 TOM70-mTURQUOISE2-SpHIS5 trp1Δ::pTDH3-mCHERRY-PTS1-CgURA3 CgLEU2-Z4EV-pZD-MSP1 ura3Δ::CgTRP1-rTA-pTET-YFP-pex15$_{\Delta C30}$-V5-tPEX15*	This study	VDY3412
S. cerevisiae: Strain *BY4741 trp1Δ::pTDH3-mCherry-PTS1::HPHMX, Pex3-GFP-AID-HIS3MX6 leu2Δ::pTDH3-OsTIR1-CgLEU2*	This study	VDY2837

S. cerevisiae: Strain *BY4741 PEX3-V5-AID-KANMX*	This study	VDY2770
S. cerevisiae: Strain *BY4741 PEX3-V5-AID-KANMX leu2Δ::pTDH3-OsTIR1-CgLEU2*	This study	VDY2773
S. cerevisiae: Strain *BY4741 PEX3-V5-AID-KANMX leu2Δ::pTDH3-OsTIR1-CgLEU2 msp1Δ::HIS*	This study	VDY3399
S. cerevisiae: Strain *PEX11-mTURQUOISE2-SpHIS5*	This study	VDY3444
S. cerevisiae: Strain *PEX11-mTURQUOISE2-SpHIS5 ura3Δ::pPEX15-sfYFP-mCHERRY-PEX15-tPEX15-KANMX*	This study	VDY3445
S. cerevisiae: Strain *PEX11-mTURQUOISE2-SpHIS5 ura3Δ::pPEX15-sfYFP-mCHERRY-PEX15-tPEX15-KANMX pex1Δ::NATMX*	This study	VDY3446
S. cerevisiae: Strain *PEX11-mTURQUOISE2-SpHIS5 ura3Δ::pPEX15-sfYFP-mCHERRY-PEX15-tPEX15-KANMX pex6Δ::URA*	This study	VDY3447